Insights into adsorbent-based pharmaceutical wastewater treatment and future developments toward sustainability

Sadia Sharmin Sporsho,†[a] Dipu Saha,†[b] Mahmudul Hasan Khan, [iD] †[b] Md Shahriar Rahman,†[b] Mahe Rukh,[b] Md Reazul Islam,[b] Tulie Chakma,[b] Faysal Haque,[c] Hridoy Roy,[b] Dipayan Sarkar [iD] [b] and Md Shahinoor Islam [iD] *[bd]

Pharmaceutical compounds have emerged as surface and groundwater contaminants over the last three decades. It is paramount to efficiently remove these contaminants from wastewater, as these molecules pose a severe threat to biodiversity and human health due to the inefficacy of wastewater treatment plants in removing many of these compounds, bioaccumulation in animal tissues, and harmful health effects caused at low concentrations. Although different removal techniques can be effective depending on the target compounds and wastewater characteristics, adsorption has a slight edge due to its low adsorbent and operational costs, high efficacy, and minimal byproducts. However, over the last decade, only a few articles have comprehensively reviewed the removal of pharmaceutical compounds through adsorption. This paper focuses on the environmental impact, detection accuracy, and effectiveness of various adsorbents for different pharmaceutical compounds. It critically analyzes the adsorption isotherms, adsorption kinetics, adsorption thermodynamics, and mechanisms of different adsorbents. Pore filling, electrostatic attraction, hydrophobic interactions, surface complexation (or bond formation), hydrogen bonding, and $\pi-\pi$ interactions are the primary mechanisms for target molecule removal during adsorption. The sustainability metrics of different adsorbents are explored for scale-up, as well as effective strategies for managing used adsorbents to support sustainability, covering the gap from the lab scale to the industrial scale.

1 Introduction

Pharmaceuticals, a significant step forward in the advancement of human scientific development, have contributed to the extension of life spans, the treatment of millions of people suffering from fatal diseases, and an overall improvement in the quality of life. Their rise to prominence as fast-expanding environmental pollutants is directly attributable to their success.[1] Almost all environmental matrices, including surface water, groundwater, and effluents and influents from wastewater treatment plants, as well as sludges and livestock industries, have been shown to contain pharmaceutical residues over the past three decades.[2–7] A few of these contaminants are so

harmful that they can interfere with human genetics, hormones, and enzymes. Pharmaceuticals, in general, have a relatively short half-life.[8–10] The body's metabolism cannot absorb the drugs entirely after humans ingest them. As a result, surplus drugs are discharged into household wastewater and subsequently enter sewage treatment facilities. Still, the reality is that many of these facilities do not consistently filter out pharmaceuticals. Both ecological systems and wastewater treatment facilities experience varying degrees of degradation, ranging from nearly complete to limited removal. Pharmaceutical residues are categorized as "compounds of emerging concern" due to their environmental persistence and potential to affect human health and ecosystems significantly.[2,11] The efficient removal of pharmaceuticals and other priority pollutants from wastewater before release is, therefore, becoming an increasingly urgent issue in the field of environmental engineering. Consequently, the prospect of removing drugs and pharmaceuticals from water is appealing to researchers, scholars, healthcare professionals, and regulatory bodies.

A wide variety of water sources have been found to contain almost every category of drugs and pharmaceuticals. Antibiotics, β-blockers, steroids, analgesics, anti-diabetics, anti-depressants, anti-epileptics, antihistamines, anti-psychotics,

[a]Department of Pharmaceutical Sciences, North South University, Dhaka 1229, Bangladesh

[b]Department of Chemical Engineering, Bangladesh University of Engineering and Technology (BUET), Dhaka-1000, Bangladesh. E-mail: shahinoorislam@che.buet.ac.bd

[c]Department of Mechanical Engineering, Bangladesh University of Engineering and Technology (BUET), Dhaka-1000, Bangladesh

[d]Department of Textile Engineering, Daffodil International University, Dhaka 1341, Bangladesh

† Co-first authors.

cytostatic, gastrointestinal, and lipid regulators are among the various types of medications and pharmaceuticals found in water.[12,13] Antibiotics receive special attention within the pharmaceutical industry due to their role in promoting the emergence and dissemination of antibiotic resistance among microorganisms, particularly pathogens, through environmental contamination. The concentrations of antiviral drugs and antibiotics (e.g., azithromycin) in wastewater sharply increased (>70%) during the pandemic.[14–16] Most of the pharmaceutical components resist contemporary wastewater treatment methods and have slow biodegradation.[17–20] It is also alarming that half of pharmaceutical wastewater is released into the environment without treatment.[21] Thus, the pollutants make their way to the domestic water body. A few of them can withstand water for an extended period. In most cases, the levels of residues from newly emerging contaminants are measured in micrograms per liter.

Pollutants in wastewater can be removed by combining physical, chemical, and biological treatment methods. Chemical treatments include coagulation, chemical oxidation, advanced oxidation, and electrochemical treatment.[22] Advanced oxidation processes (AOPs) are suitable for removing chloroquine,[23] ivermectin,[24] azithromycin,[24] penicillin,[25] diclofenac,[26] ciprofloxacin, and paracetamol.[27] However, these removal processes are primarily laboratory-based and costly. Chemical oxidation and electrochemical processes may form byproducts that might be more harmful and toxic than the primary compounds in wastewater. Biological treatments are ineffective and slow processes, as antibiotics are difficult for microorganisms to degrade. The physical treatment methods incorporate sedimentation, sand filtration, adsorption, and membrane treatments.[28] Physical wastewater treatment facilities, such as sedimentation and sand filtration, cannot fully degrade pharmaceuticals due to their design, which typically handles organics in the mg L^{-1} range. Membrane treatments are highly effective in removing pharmaceutical compounds; however, cost, clogging, and the need for frequent cleaning are the major issues associated with these treatments. Nano-filtration can remove up to 85% of anti-inflammatory drugs from wastewater.[28] Several downsides are associated with most systems, including time consumption, rigorous operating specifications, cost, and periodic maintenance.[29–32] Considering these drawbacks, the adsorption technique is highly utilized due to its low cost, ease of operation, efficacy, and stability in removing pharmaceutical waste.[30–33] Fig. 1 presents the number of articles published recently with keywords related to adsorption and pharmaceutical wastewater.

Many kinds and categories of adsorbents have emerged from the macro-to the nanoscale in recent years. Fig. 2 presents a schematic overview of the principal approaches for treating pharmaceutical wastewater. The advantages of adsorbents are their small size, great potential for tuning according to needs, large surface area per unit mass, existence of multiple active sites, and high effectiveness in removing pollutants.[34]

The high binding capacity of adsorbents for pharmaceuticals has made adsorption a valuable method for purifying pharmaceutical effluents. Adsorption has shown potential for
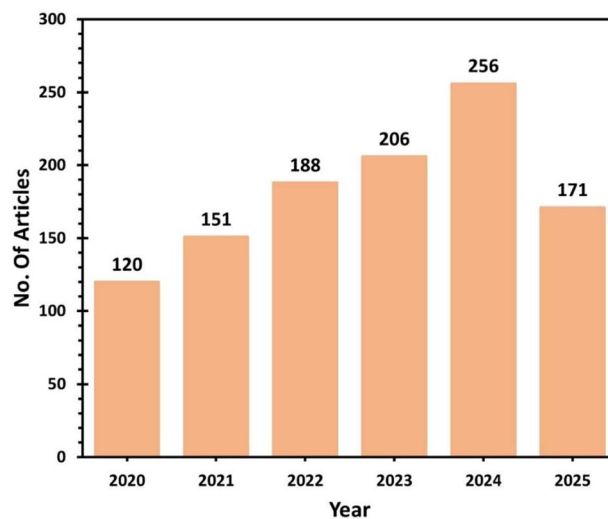

Fig. 1 Recently published articles on adsorption and pharmaceutical wastewater from 2020–2025 (language limited to English). Source: Scopus.

pharmaceutical removal from water and effluents to prevent pollution and waste handling because of its straightforward design, easy operation, and absence of unwanted byproducts.[35] Furthermore, the cost of treating wastewater using adsorption can be comparable to other techniques, such as the advanced oxidation process, depending on the pollutants and employed technique.[36–38] Recently, numerous studies have removed pharmaceuticals from wastewater using various adsorbents, including activated carbon, biochar, porous carbon, zeolite, MOF, graphene, polymer, perovskite, etc.[35,39,40] Features of the pollutants, such as charge, shape, size, and solubility, greatly influence the binding of pollutant species to an adsorbent surface. Adsorbent-based pharmaceutical treatment has a facile design and requires less energy than the advanced oxidation process to remove pharmaceuticals.[41–43] Advanced oxidation processes can produce toxic byproducts during operation, making it difficult to scale up.[41,43] On the other hand, adsorbent-based treatment methods are easier to scale and modify for use in real-world applications. Adsorption-based pharmaceutical wastewater treatments are available in real-world applications. The most common companies are DESOTEC, HYERA INC., and NORIT, and they utilize activated carbon as an adsorbent, either in powdered or granular form, to remove pharmaceuticals.[44–46]

Several publications on degrading and removing pharmaceutical substances have recently appeared in top peer-reviewed journals. However, only a few published studies have detailed the use of adsorbents to remove these compounds. In this article, a comprehensive approach was taken to review the current state-of-the-art methods using next-generation adsorbents to remove emerging pharmaceutical contaminants, as well as future remedial methods available to achieve these treatments in a more eco-friendly and sustainable manner. The article also explores the adsorption isotherms, kinetics, and mechanisms of pharmaceutical waste removal.
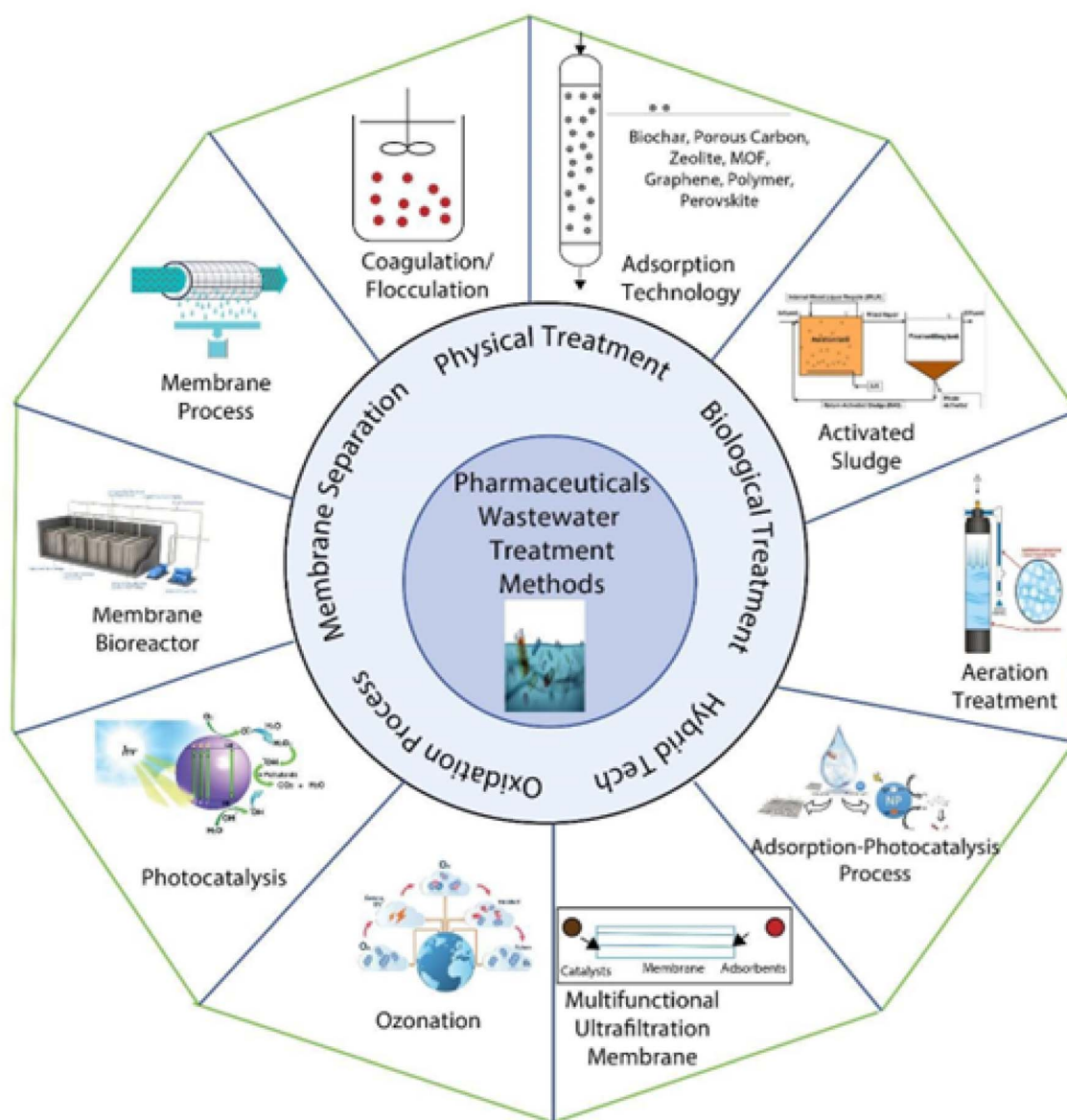
Fig. 2 A graphical overview of pharmaceutical wastewater treatment methods.

2 Pharmaceutical wastewater characteristics

Pharmaceutical wastewater (PW) is a complex array of organic and inorganic molecules with varying physicochemical properties.[47,48] The success of any PW treatment process depends on understanding the physicochemical properties of the target compound and the wastewater and designing the process accordingly.[49] Parameters, including pH, initial pollutant concentration, pollutant hydrophobicity, treatment time, and temperature, considerably influence the adsorption of wastewater pollutants.[50]

A wide range of pH values, from 3.7 to 14, has been reported in various studies for different PWs (Table 1). Understanding the correlation between the pH and the pollutant can be crucial

for efficient wastewater treatment. Like other pollutants, pharmaceutical pollutants (PP) are present in their ionic form in wastewater. The zeta potential (ZP) value indicates the electrostatic interaction between a charged surface and PP. The variation of ZP of PP is influenced by the pH of the solution, which affects the PP removal kinetics and mechanism.[51] Chemical oxygen demand (COD) and biochemical oxygen demand (BOD) are the main water quality parameters. The typical COD and BOD content in wastewater from pharmaceutical manufacturing industries ranges between 800 and 60 000 mg L^{-1} and 40 and 21 560 mg L^{-1}, respectively (Table 1).

The most frequently detected active pharmaceutical ingredients (APIs) in wastewater are blood lipid regulators, non-steroidal anti-inflammatory drugs (NSAIDs), antibiotics, selective serotonin reuptake inhibitors (SSRIs), analgesics, β-blockers, hormones, and antihistamines.[52] Kostich *et al.*[53]

Table 1 Physicochemical properties of PW from different sources

Manufacturing type	Main API	Main API concentration (mg L^{-1})	COD (mg L^{-1})	BOD$_5$ (mg L^{-1})	TOC (mg L^{-1})	NH$_3$-N (mg L^{-1})	pH	TSS (mg L^{-1})	TDS (mg L^{-1})	NO$_3^-$ (mg L^{-1})	PO$_4^{3-}$ (mg L^{-1})	Reference
Formulation facility	Carbamazepine Venlafaxine	0.84 (±0.19) 11.72 (±2.2)	4765 (±1405)	634 (±100)	1698 (±308)	23.5 (±8)	10.2 (±0.9)	NS	NS	NS	NS	56
Manufacturing industry	Paracetamol	48	3500	466	NS	NS	6.8	360	600	NS	NS	57
Bulk manufacturing unit	NS	NS	37 410 (±225)	21 560 (±160)	8250 (±145)	NS		6780 (±180)	21 340 (±450)	18 (±1.25)	0.2 (±0.03)	58
Bulk manufacturing unit	Antibiotic	NS	15 365 (±1214)	NS	7624 (±710)	NS	7–8	388 (±87)	22 168 (±3757)	NS	NS	59
Chemical synthesis	Antibiotic	NS	16 249 (±714)	NS	6697 (±1047)	NS	7–8	199 (±59)	29 450 (±1209)	NS	188 (±29)	60
Chemical synthesis	Etodolac	50–215	20 000–23000	NS	NS	NS	3.7–11.3	NS	NS	30–34^a	0.5–2.2^b	61
Manufacturing and equipment cleaning	Penicillin Triethylamine	NS 9872 (±2142)	16 547 (±1827)	10 184 (±2574)	8083 (±578)	72 (±46)	7–9	285 (±175)	24 899 (±1758)	NS	NS	47
Chemical synthesis	Antibiotic	NS	39 000–60000	NS	NS	NS	7–8	800–1000	NS	NS	3–6^c	62
Hospital water treatment plant	NS	NS	376	NS	NS	22.3^d	7–7.5	NS	NS	0.2	NS	63
Chemical synthesis	Diclofenac Chlorophenol	18–20 <3	500–593.53	NS	170.76–200	NS	7–7.14	NS	NS	NS	NS	64
Wastewater treatment plant	NS	NS	1800	1130	NS	NS	7.5	750	NS	NS	16	52
Pharmaceutical industry	NS	NS	810	40	NS	NS	7.27	118	NS	7.23	2.13	65
Hospital wastewater	NS	NS	918	400	220	46	7.7	310	NS	NS	7.4	65
Fermentation-based PW	NS	NS	6800.5	>2040	2476.3	50.7	NS	188.3	NS	NS	NS	66

^{a} NO$_3$-N. ^{b} Total phosphate. ^{c} PO$_4$-P. ^{d} NH$_4^+$; NS: not studied.

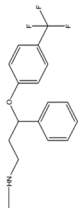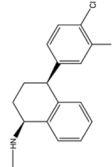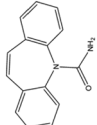**Table 2** Ecotoxicological effects of different active pharmaceutical ingredients on various organisms
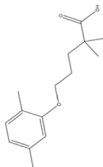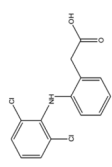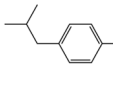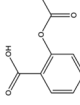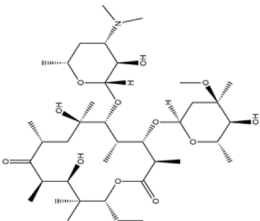
Active ingredient	Structure	Classification	Organism	Lethal concentration, 50% (LC$_{50}$) (mg L^{-1})	Effective concentration, 50% (EC$_{50}$) (mg L^{-1})	Effect	Reference
Fluoxetine		Selective serotonin reuptake inhibitor (SSRI)	*Oryzias javanicus*	1.23 (96 h)	0.01 (96 h, swimming behavior)	Decreased swimming performance, disruption of the endocrine system, DNA damage, and oxidative and endoplasmic reticulum stress	69
			Hydra magnipapillata	2.90 (72 h)		Reduced reproduction, morphological deformation, neurotransmission disturbance, DNA damage, and oxidative stress	
Sertraline		SRRI	*Daphnia magna*	0.12 (21 days)	0.06 (21 days, reproduction)	Increased mortality and reduced reproduction	70
Carbamazepine		Anticonvulsant	*Oncorhynchus mykiss*			Two-fold reduction of intestinal RNA/DNA ratio, induced oxidative stress, and disrupted osmoregulation	71
Gemfibrozil		Blood lipid regulator	*Danio rerio* larvae	11.01 (96 h)		Increased hatching time, reduced hatchability, locomotion impairment, edema formation, and yolk sac malformation	72
Diclofenac		Non-steroidal anti-inflammatory drug (NSAID)	*Mytilus galloprovincialis*			DNA damage, oxidative stress, lipid metabolism disorder, and osmoregulation disruption	73
Ibuprofen		NSAID	*Planorbis carinatus* *Dreissena polymorpha*	17.1 (72 h)		Decrease in growth Induction of oxidative stress and exhibited genotoxic effects	74 57
Aspirin		NSAID	*Daphnia*		86.1 (48 h, daphnid immobilization)	DNA damage, deformities in neonates, behavioral and physiological changes, induction of oxidative stress, and reduced reproduction	75

Table 2 (Contd.)

Active ingredient	Structure	Classification	Organism	Lethal concentration, 50% (LC$_{50}$) (mg L^{-1})	Effective concentration, 50% (EC$_{50}$) (mg L^{-1})	Effect	Reference
Erythromycin		Antibiotic	Oncorhynchus mykiss			Gill: vasodilation, oedema, epithelial lifting, lamellar epithelial desquamation, lamellar fusion, hyperplasia on the epithelium of the gill. Liver: increase in sinusoidal space, hemorrhage, cytoplasmic vacuolization, nuclear degeneration, and nuclear/cellular hypertrophy of hepatocytes	76

investigated the effluents of the 50 largest wastewater treatment plants in the US and reported 56 APIs present in various concentrations. Among these APIs, the most detected ones (30 detections) are atorvastatin, carbamazepine, ciprofloxacin, diltiazem, furosemide, diltiazem-desmethyl, gemfibrozil, hydrochlorothiazide, metoprolol, ofloxacin, oxycodone, propranolol, sertraline, sulfamethoxazole, triamterene, trimethoprim, valsartan, and verapamil. Valsartan was found to have the highest maximum concentration of 5300 ng L^{-1}, followed by ibuprofen (4200 ng L^{-1}), lisinopril (3300 ng L^{-1}), atenolol (3000 ng L^{-1}), sulfamethoxazole (2900 ng L^{-1}), hydrochlorothiazide (2800 ng L^{-1}), and gemfibrozil (2300 ng L^{-1}). The USGS surveyed 1091 sites spanning 46 states to assess the pharmaceutical and hormone content of groundwater from 2013 to 2015.[54] 1,7-dimethylxanthine, carbamazepine, meprobamate, sulfamethoxazole, and bisphenol A showed the highest number of detections (more than 0.5%) with detection counts of 9, 18, 8, 12, and 7, respectively. This study revealed that principal aquifers in the USA have already been contaminated with pharmaceutical and hormone compounds, although at levels below safety benchmarks for humans. Another USGS survey was conducted (2014–2017) on 308 wadable streams across four regions of the USA to measure 108 pharmaceutical analytes.[55] Compounds detected in the most significant number of sites were nicotine (70% sites), metformin (68% sites), cotinine (47% sites), lidocaine (42% sites), caffeine (42% sites), carbamazepine (41% sites), and acetaminophen (26% sites).

3 Ecotoxicological impact of pharmaceutical compounds

The effect of pharmaceutical compounds on organisms depends on the organism type and class, exposure time, and physicochemical properties of pollutants and the environment (i.e., water).[49] Pharmaceutical pollutants (PPs) can be absorbed and bioaccumulate in living organisms through ingestion (from food and drinking water), respiration, and other uptake methods (e.g., dermal absorption). This subsection focuses on the ecotoxicological effects of different pharmaceutical components on aquatic organisms.

The various active ingredients of pharmaceutical pollutants have a significant impact on aquatic organisms, posing a severe threat to their aquatic life. The ecotoxicological impact of pharmaceutical compounds on different organisms is summarized in Table 2. The literature review in this section highlights the severe threat different pollutants pose to aquatic creatures. Although most of the work reviewed here does not represent environmentally relevant conditions, the bioaccumulation capabilities of these pollutants can potentially create similar complications under low pollutant concentrations. Therefore, we need to understand various wastewater treatment techniques and implement effective methods to minimize potential environmental damage.

Pharmaceuticals, including antibiotics, hormones, and analgesics, are increasingly being detected in water bodies, disrupting aquatic ecosystems and contributing to issues like

antimicrobial resistance (AMR).[67] An adsorption system has been successfully demonstrated for removing pharmaceuticals from real wastewater using low-cost sorbents in a pilot-scale plant.[68] The cost-effective nature and exceptional performance of the adsorption technique provide a distinct advantage over traditional methods. Therefore, the primary objective of this review is to investigate the role of adsorbents in removing pharmaceuticals from aquatic systems.

4 Important adsorption parameters for pharmaceutical wastewater treatment

Adsorption has emerged as a promising approach for treating pharmaceutical wastewater; however, its application remains relatively limited, despite the availability of a diverse range of adsorbents. Traditional materials such as zeolites, activated carbon, and carbon nanomaterials have been extensively investigated. In contrast, novel adsorbents, including metal–organic frameworks (MOFs), graphene-based materials, carbonaceous compounds, polymeric materials, metal oxide nanoparticles, biochar, and sustainable materials, are being increasingly explored for their potential. Fundamental parameters, such as adsorption isotherms and kinetics, govern the adsorption of various pharmaceutical pollutants onto different adsorbents. However, their performance can vary significantly due to the differences in material properties, surface characteristics, and experimental conditions. This section provides an in-depth discussion of the key adsorption features, including the adsorption isotherms, adsorption kinetic models, and potential adsorption mechanisms of different adsorbents in removing various pharmaceutical pollutants.

4.1 Adsorption kinetics model

Reaction kinetics describe the rate at which a reaction occurs and identify the factors influencing this rate. In the case of porous adsorbents, adsorption equilibrium is typically not achieved instantly. The kinetic study examines the adsorption rate, which can be influenced by varying mass-transfer conditions depending on the pressure, the temperature, and the properties of both the adsorbate and adsorbent. The solid material encounters two primary resistances: (i) external diffusion resistance, which refers to mass transfer from the bulk fluid to the external surface of the adsorbent, and (ii) intraparticle diffusion resistance, which involves mass transfer from the external surface to the interior pore of the adsorbent. Adsorption kinetics can be determined using mathematical models, with the pseudo-first-order and pseudo-second-order models being the most frequently used.[77] Mechanistic adsorption typically proceeds *via* multi-step pathways, beginning with film diffusion, surface binding, and intraparticle diffusion. Such processes can be evaluated using the Weber–Morris and Boyd models, which provide insight into whether adsorption is surface- or diffusion-limited.

4.2 Adsorption isotherm model

Adsorption isotherm models define the relationship between the amount of adsorbate adsorbed per unit mass of adsorbent at equilibrium and its concentration in the surrounding phase (liquid or gas). The variations in adsorption isotherms provide valuable insights into the interactions between the adsorbent and adsorbate. Additionally, these isotherms help determine the adsorbent's pore structure and specific surface area. Consequently, analyzing adsorption isotherms and developing models are essential for understanding and optimizing the adsorption process to achieve maximum efficiency. The most used adsorption isotherm models for pharmaceutical wastewater treatment are the Langmuir and Freundlich models. Incorporating the Temkin and Dubinin–Radushkevich models enables the evaluation of adsorption energetics, revealing whether physical or chemical interactions dominate uptake. Multi-layer models, such as Sips and Redlich–Peterson, better describe adsorption on heterogeneous and high-surface-area adsorbents, including MOFs and graphene composites. Table 3 indicates commonly used kinetic and isotherm models for the pharmaceutical adsorption process.

4.3 Thermodynamics of adsorption

Since motion is an intrinsic property of matter and energy is inherently associated with this motion, it is natural that physical and chemical transformations involve energy changes. Thermodynamics, a branch of physical science, examines these energy variations. Key thermodynamic parameters—Gibbs free energy (ΔG), enthalpy (ΔH), and entropy (ΔS)—offer valuable insights into a material's adsorption capacity. These parameters are crucial for understanding adsorption mechanisms, as they help determine the feasibility, spontaneity, and heat exchange associated with the process.

4.4 Fixed-bed adsorption and dynamic modeling for industrial applications

While batch adsorption studies are widely used to evaluate the capacity and mechanisms of adsorbents, they provide limited insight for industrial-scale applications, where continuous operation and predictive modeling are essential. Fixed-bed column adsorption represents the most practical and scalable configuration for wastewater treatment because it can operate continuously, achieve high throughput, and facilitate straightforward adsorbent regeneration. Unlike batch systems, fixed-bed columns capture breakthrough behavior, service time, and mass-transfer limitations, which are critical for process design and scale-up.

The adsorption performance in fixed-bed systems is typically evaluated using dynamic modeling, which predicts breakthrough curves and service life under realistic flow conditions. Among the widely used models, the Thomas, Bohart–Adams, and Yoon–Nelson equations are the most common due to their simplicity, robust applicability, and ability to guide industrial-scale column design.

Table 3 Commonly used kinetic and isotherm models for the pharmaceutical adsorption process[a] [78–86]

Adsorption kinetics model	Linear form	Non-linear form	Application insights	Adsorption isotherm model	Linear form	Non-linear form	Application insights
Pseudo-first-order model (Lagergren model)	$\ln(q_e - q_t) = \ln q_e - k_1 t$	$q_t = q_e(1 - e^{-k1t})$	Describes initial rapid adsorption; suitable for low-concentration or early-time studies	Langmuir model	$C_e/q_e = q/(K_L\,q_L) + C_e/q_L$	$q_e = \dfrac{q_m K_L C_e}{1 + K_L C_e}$	Estimates maximum adsorption capacity (q_{max}); guides adsorbent dosage and saturation prediction
Pseudo-second-order model	$t/q_t = 1/(k_2 q_e{}^2) + t/q_e$	$q_t = \dfrac{q_e{}^2 k_2 t}{1 + q_e k_2 t}$	Predicts overall adsorption capacity and equilibrium; widely used for pharmaceutical uptake	Freundlich model	$\ln q_e = \ln K_F + (1/n)\ln C_e$	$q_e = K_F C_e{}^{\frac{1}{n}}$	Evaluates surface heterogeneity; predicts adsorption intensity in multi-contaminant wastewater
Intraparticle diffusion model (Weber–Morris model)	$q_t = k_i t^{1/2} + c$	—	Identifies pore-diffusion control and multi-stage adsorption, important for porous adsorbents	Dubinin–Radushkevich (D–R) model	$\ln q_e = \ln q_D - K_{DR}\varepsilon^2$	$q_e = q_D e^{-K_{DR}\varepsilon^2}$, $\varepsilon = RT\ln\dfrac{C_s}{C_e}$	Distinguishes physisorption (<8 kJ mol^{-1}) and chemisorption; indicates regeneration feasibility
Pore-diffusion model	$\log q_t = k \log t$	—	Distinguishes film-controlled vs. diffusion-controlled processes	Redlich–Peterson model	$\ln\left(K_{RP}\dfrac{C_e}{q_e} - 1\right) = \ln(\alpha_{RP}) + \beta\ln(C_e)$	$q_e = \dfrac{K_{RP} C_e}{1 + \alpha_{RP} C_e{}^\beta}$	Provides accurate fits for real systems; useful for industrial-scale predictions
Elovich model	$q_t = \dfrac{1}{\beta}\ln(1 + \alpha\beta_t)$	—	Explains non-uniform surface energy adsorption; useful for biochar and metal-doped adsorbents	Temkin model	$q_e = \dfrac{RT}{b}\ln A + \dfrac{RT}{b}\ln C_e$	$q_e = \dfrac{RT}{b}\ln(A C_e)$	Indicates chemisorption on heterogeneous surfaces
Boyd's film diffusion model	$B_t = \{2\pi - \dfrac{\pi^2 F(t)}{3}$ $-2\pi(1 - \pi F(t)/3)^{\frac{1}{2}}$; $(0 < F(t) < 0.85)$ $-0.4977 - \ln(1 - F(t))$; $(0.86 < F(t) < 1)\}$	$F = 1 - \dfrac{6}{\pi^2}$ $\sum\dfrac{1}{n^2}\exp(-n^2 B_t)$	Distinguishes film-controlled vs. particle-controlled adsorption, key for column scale-up	Sips model	$\ln\left(\dfrac{q_e}{q_{ms} - q_e}\right) =$ $\dfrac{1}{n_s}\ln(C_e) + \ln(K)^{\frac{1}{n_s}}$	$q_e = \dfrac{q_{ms} K_s C_e{}^{n_s}}{1 + K_s C_e{}^{n_s}}$	Ideal for heterogeneous, multi-site adsorbents; effective across low and high concentration ranges

[a] Note: t is the adsorption time (min), q_t (mg g^{-1}) is the adsorbed amount of the adsorbate at time t, q_e is the adsorption capacity at equilibrium (mg g^{-1}), k_1 is the pseudo-first-order rate constant (min^{-1}), k_2 is the pseudo-second-order rate constant (g mg^{-1} min^{-1}), k_i (mg g^{-1} min$^{-1/2}$) is the rate constant of the intraparticle diffusion model, c is the degree of diffusion, α (mg g^{-1} min^{-1}) is the primary rate of adsorption, β represents the desorption parameter in the Elovich model, B_t is a parameter relating to adsorbent characteristics, $F(t)$ is defined as q_t/q_e, K_F (L$^{1/n}$ mg$^{1-1/n}$ g^{-1}) is the Freundlich constant, n is the dimensionless Freundlich intensity parameter, K_{DR} is the D–R constant related to the mean free energy of adsorption, ε is the adsorption potential, K_{RP} is the Redlich–Peterson constant, which is related to the adsorption capacity, α_{RP} is the Redlich–Peterson constant, related to the adsorption intensity, β is an exponent that lies between 0 and 1, A is the Temkin isotherm equilibrium binding constant (L g^{-1}), which is related to the maximum binding energy, q_{ms} (mg g^{-1}) is the maximum adsorbed amount, K_s (L^{n_s} mg$^{-n_s}$), and n_s is the Sips constant.

Thomas model: The Thomas model assumes plug-flow behavior with second-order reversible kinetics and negligible axial dispersion. It is widely applied to predict adsorption capacity, breakthrough curves, and bed exhaustion times. The model is given by:

$$\ln\left(\frac{C_0}{C_T} - 1\right) = k_{Th} q_0 \frac{m}{Q} - k_{Th} C_0 t$$

where C_0 and C_t are the inlet and outlet concentrations (mg L^{-1}), q_0 is the maximum adsorption capacity (mg g^{-1}), k_{Th} is the Thomas rate constant (L mg^{-1} min^{-1}), m is the adsorbent mass (g), and Q is the volumetric flow rate (L min^{-1}).

Bohart–Adams model: The Bohart–Adams model correlates column performance with bed depth and service time, assuming that adsorption is primarily controlled by surface reaction kinetics. It is beneficial for estimating bed depth requirements, service time, and early breakthrough performance. The linearized form is:

$$\ln\frac{C_t}{C_0} = k_{BA} N_0 \frac{Z}{U} - k_{BA} C_0 t$$

where k_{BA} is the kinetic constant (L mg^{-1} min^{-1}), N_0 is the saturation concentration (mg L^{-1}), Z is the bed depth (cm), and U is the superficial velocity (cm min^{-1}).

Yoon–Nelson model: The Yoon–Nelson model simplifies column design by assuming that the adsorbate breakthrough probability is directly proportional to the adsorption rate. This model predicts the time for 50% breakthrough (τ) without requiring extensive parameter fitting:

$$\ln\left(\frac{C_t}{C_0 - C_t}\right) = k_{YN}(t - \tau)$$

where k_{YN} is the Yoon–Nelson rate constant (min^{-1}), and τ is the time required for 50% breakthrough (min).

4.5 Adsorption mechanism

Adsorption refers to the selective attachment of a specific ion or compound at the interface between two distinct phases. When occurring on a solid surface, adsorption can be categorized as physical adsorption (physisorption) or chemical adsorption (chemisorption). Physisorption arises from intermolecular forces, including induced dipoles, permanent dipoles, secondary valence forces, and van der Waals interactions. It is generally reversible, less specific, and associated with low thermal effects. Physical adsorption (physisorption) is predominantly regulated by weak, non-covalent interactions, including van der Waals forces, electrostatic attractions, hydrogen bonding, π–π stacking, and hydrophobic effects. These interactions are often non-specific and reversible, facilitating swift initial absorption without modifying the chemical structure of either the pharmaceutical adsorbate or the adsorbent. Physisorption is generally characterized by low adsorption energies, ranging from 4 to 40 kJ mol^{-1}, which promotes adsorption–desorption cycles and the renewal of adsorbents.[87,88] Hydrophobic interactions significantly influence aqueous environments, where nonpolar drugs tend to associate with hydrophobic surfaces to reduce contact with water molecules.

Chemisorption, in contrast, occurs when the adsorbate and adsorbent share electrons, forming strong valence bonds. This adsorption type is typically irreversible, highly selective, and characterized by significant thermal effects. Chemisorption is characterized by elevated adsorption energies, typically ranging from 80 to 400 kJ mol^{-1}, and often results in structural changes in the adsorbate or the formation of stable surface complexes. Principal chemisorption mechanisms encompass ion-pair and electron–transfer interactions between charged pharmaceutical entities and active surface sites, surface complexation and coordinate bonding at metal centers, ion exchange, and, in certain instances, redox reactions that augment binding or initiate partial transformation of the pollutant.[87,88] Robust and selective interactions are essential for the elimination of persistent and low-concentration medicines from intricate aqueous matrices. Analyzing the adsorption mechanism provides substantial insight into the efficacy of various adsorbents for different pharmaceutical adsorbates. This review thoroughly explores the interactions between pharmaceutical pollutants and adsorbents during the adsorption process. The adsorption of pharmaceutical micro-contaminants onto an adsorbent surface primarily occurs due to surface energy, as the atoms or functional groups on the adsorbent attract the adsorbate to minimize surface energy. The adsorption mechanism is significantly influenced by ambient and material variables, including pH, ionic strength, surface charge, and the type and density of surface functional groups. Functional groups like –OH, –NH$_2$, –COOH, and –C=O promote hydrogen bonding, ion exchange, and coordination with medicinal compounds, while the hydrophilicity or hydrophobicity of the adsorbent surface determines its affinity for polar or nonpolar pollutants. The pH of the solution regulates the ionization of both adsorbates and adsorbent surfaces; therefore, it directly influences electrostatic and ion-pair interactions. The existence of concurrent ions or natural organic materials can also influence adsorption mechanisms by competing for active sites or obstructing electrostatic interactions. The driving force behind adsorption results from the combined effect of multiple interactions that contribute to the total free energy of the process. These interactions include hydrogen bonding, electrostatic attraction, π–π interactions, and dipole–dipole interactions between the adsorbent and adsorbate.[89] In certain instances, van der Waals forces and hydrophobic interactions contribute to the adsorption of organic molecules onto adsorbent materials. Van der Waals forces refer to intermolecular attractions, categorized as weak London dispersion forces and stronger dipole–dipole interactions. Another possible binding mechanism for pharmaceutical contaminants is the hydrophobic interaction between nonpolar groups. In contrast to intermolecular forces, hydrophobic interactions are driven by entropy, resulting from the exclusion of chemicals from the aqueous phase rather than a direct attraction to the adsorbent. The potential adsorption mechanisms of aqueous pharmaceuticals onto various adsorbents are summarized in Fig. 3.
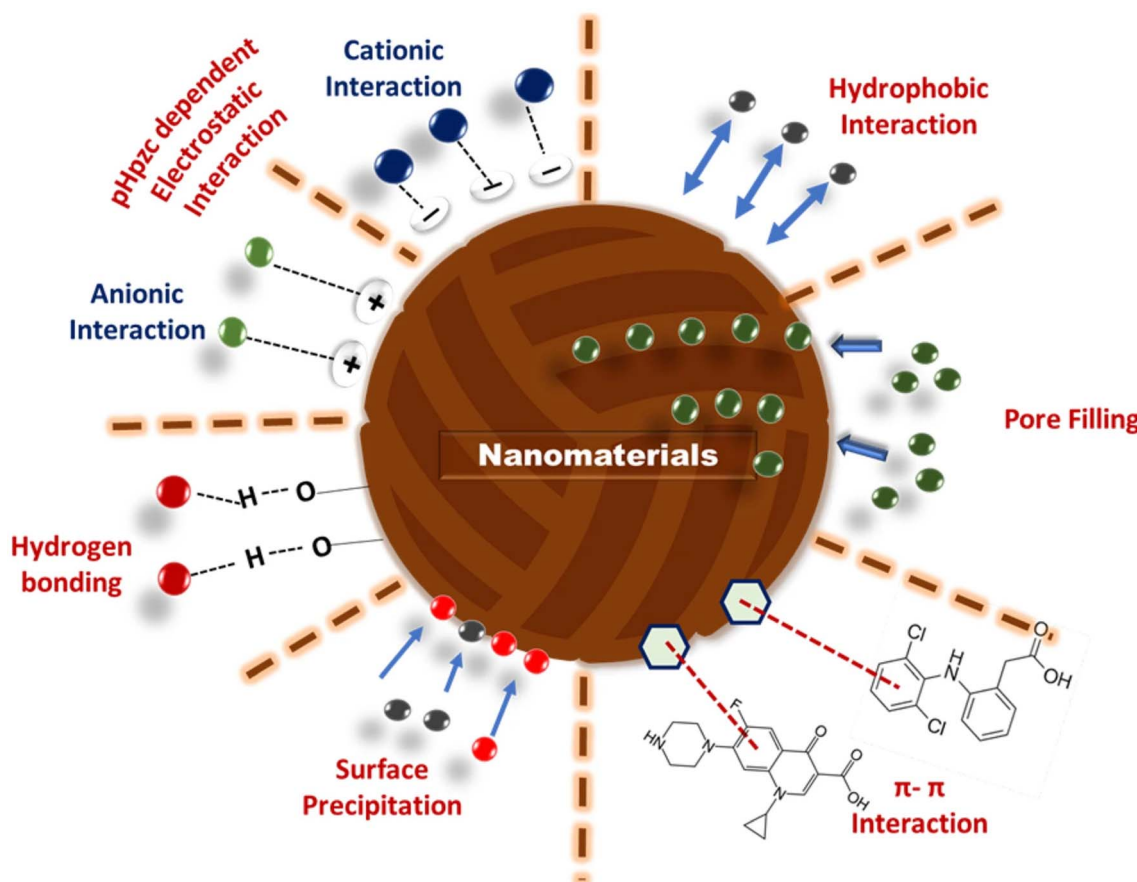
Fig. 3   Potential mechanisms behind the adsorption of pharmaceuticals onto nanoparticles (adapted from ref. 90 with permission from Springer Nature, copyright 2023).

5   Performance of adsorbents in removing pharmaceutical pollutants

Adsorption is a highly viable technique for removing micro-pollutants due to its ease of setup and cost-effectiveness. This method has been commonly applied to eliminate natural and synthetic organic compounds from wastewater. Here, we present a detailed discussion of the performance and efficacy of various adsorbents in removing pharmaceutical pollutants.

5.1   Zeolite

In recent years, research has been focusing on incorporating zeolites to remove specific compounds and organic micro-pollutants in pharmaceutical wastewater. Zeolites are micro-porous minerals that mainly contain aluminum and silica compounds, used as commercial adsorbents and catalysts.[91] More than 40 naturally occurring zeolites and more than 253 unique zeolite frameworks have been discovered. The framework of zeolites is composed of tetrahedral units of silica and alumina, which possess high porosity, a large surface area, and good physical and chemical properties, enabling them to remove emerging pollutants from pharmaceutical wastewater.

Izzo *et al.* successfully modified natural zeolites using long-chain cationic surfactants to develop a composite material with a high adsorption capacity for ibuprofen.[92] Martucci *et al.* investigated the adsorption capacity for the removal of erythromycin, carbamazepine, and levofloxacin drugs from pharmaceutical wastewater using three organophilic zeolites (Y, mordenite (MOR), ZSM-5).[93] Zeolite Y (dealuminated faujasite) was studied by Braschi *et al.* and confirmed to effectively remove sulfonamide antibiotics from water, which significantly contribute to bacterial resistance.[94] The adsorptive removal of norfloxacin (NOR) and ofloxacin (OFL) was explored by Zhao *et al.* using a polyethylene glycol (PEG-4000) surfactant-modified and zeolite-supported nanoscale zero-valent iron composite.[95] Fig. 4 shows the various steps involved in the synthesis, characterization, and removal mechanism of two antibiotics with PZ-NZVI composite. Within one hour, more than 95% of NOR or OFL could be removed from the solution using PZ-NZVI, and the adsorption process could be best described using the pseudo-second-order kinetic model and the Temkin isotherm model. The characterization results before and after adsorption, as well as batch studies, demonstrated that various processes, including hydrophobic interaction, bi-dentate complex formation between Fe and fluoroquinolones, pore filling, and electrostatic interaction, can control the sorption process.

Arabkhani *et al.* reported an ultra-high adsorption capacity value of 2594 mg g^{-1} at 30 °C for the removal of diclofenac
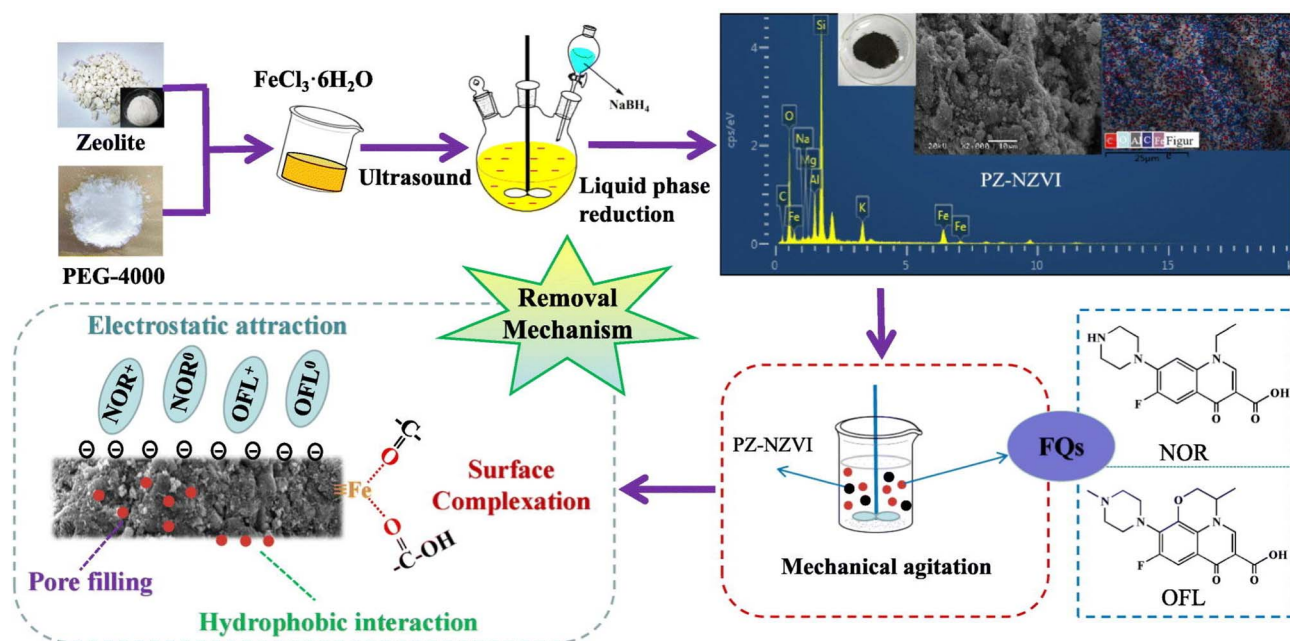
Fig. 4 A graphical representation of removing two fluoroquinolone antibiotics (NOR: naproxen and OFL: ofloxacin) using PEG-4000-stabilized nanoscale zero-valent iron supported on zeolite (PZ-NZVI) (adapted from ref. 95 with permission from Elsevier, copyright 2020).

sodium from pharmaceutical wastewater by synthesizing graphene oxide (GO) nanosheets with zeolitic imidazolate framework-8 (ZIF-8), pseudo-boehmite (γ-AlOOH), and iron oxide (Fe_3O_4) nanoparticles.[96] Liu *et al.* confirmed that modified zeolite-supported nano-MoS_2 (MoS_2@zeolite) with multiple adsorption sites is an efficient and promising adsorbent for treating pharmaceutical wastewater tetracycline.[97] Attia *et al.* synthesized magnetic nanoparticles coated with zeolite (MNCZ) to adsorb medicinal substances from pharmaceutical compounds.[98] Hexadecyltrimethylammonium (HDTMA)-modified zeolites showed hydrophobic interaction mechanisms when estrogenic contaminants were removed from wastewater.[99] Thus, adsorbents based on zeolites and nanocomposites might be promising next-generation adsorbent materials for treating pharmaceutical wastewater; however, continuous operation will not eliminate the need for regular adsorbent material replacement and regeneration.

5.2 Metal–organic frameworks (MOFs)

Metal–organic frameworks (MOF) are unique three-dimensional (3D) functional hybrid materials with extremely porous nanostructures that can be synthesized by linking metal-containing ions/groups and organic linkers through strong bonds (reticular synthesis). A MOF is essentially a crystalline structure with persistent porosity (usually more than 50% of the crystal volume), and the typical surface area of MOFs varies from 1000–10,000 m^2 g^{-1}, much higher than those of zeolites and carbons. MOFs have been intensively studied for decades, and appropriately designed examples have emerged as some of the magnetic materials of choice for scientists and inventors due to the presence of promising components with tunable pore networks, their flexibility and varying sizes, and an abundance of adsorption sites, among other features.

MIL-101 (chromium–benzene dicarboxylate), in which MIL stands for Material of Institute Lavoisier, is one of several MOFs created so far that have been extensively studied for prospective use for the removal of naproxen and clofibric acid from wastewater due to its very high porosity (1.9 cm^3 g^{-1}). Hasan *et al.* further functionalized MIL-101 with an acidic group (AMSA-MIL-101) and a primary group (ED-MIL-101). They conducted batch experiments to explore the adsorption effectiveness of eliminating naproxen and clofibric acid.[100] UiO-66 with controlled defects contained more open frameworks and showed a higher affinity for diclofenac than other pharmaceuticals.[101] Methanol-activated Cu-based MOF(HKUST-1) showed excellent adsorption capacity to remove sulfonamide antibiotics and sulfachloropyridazine (SCP).[102] The high surface area, large pore volume, and unsaturated metal sites resulted in faster, spontaneous, and endothermic adsorption kinetics for removing sulfonamide antibiotics. Fig. 5 shows that electrostatic interactions, H-bonding interaction with the H of the NH_2 from the SCP and the oxygen of the HKUST-1 clusters, and π–π stacking between the benzene ring of the MOF and the SCP are primarily responsible for the high adsorption capacity.

Lu *et al.* fabricated a novel amino-functionalized aluminum-based metal–organic framework (Al-MOF@NH_2), demonstrating high hydrocortisone (HC) adsorption capacity, a common steroid hormone drug. Large-scale manufacturing, water stability, and reusability are three critical obstacles to using MOFs as adsorbents. Most MOFs are not water stable, which may lead to poor recovery and even second-hand pollution from metal leaching.
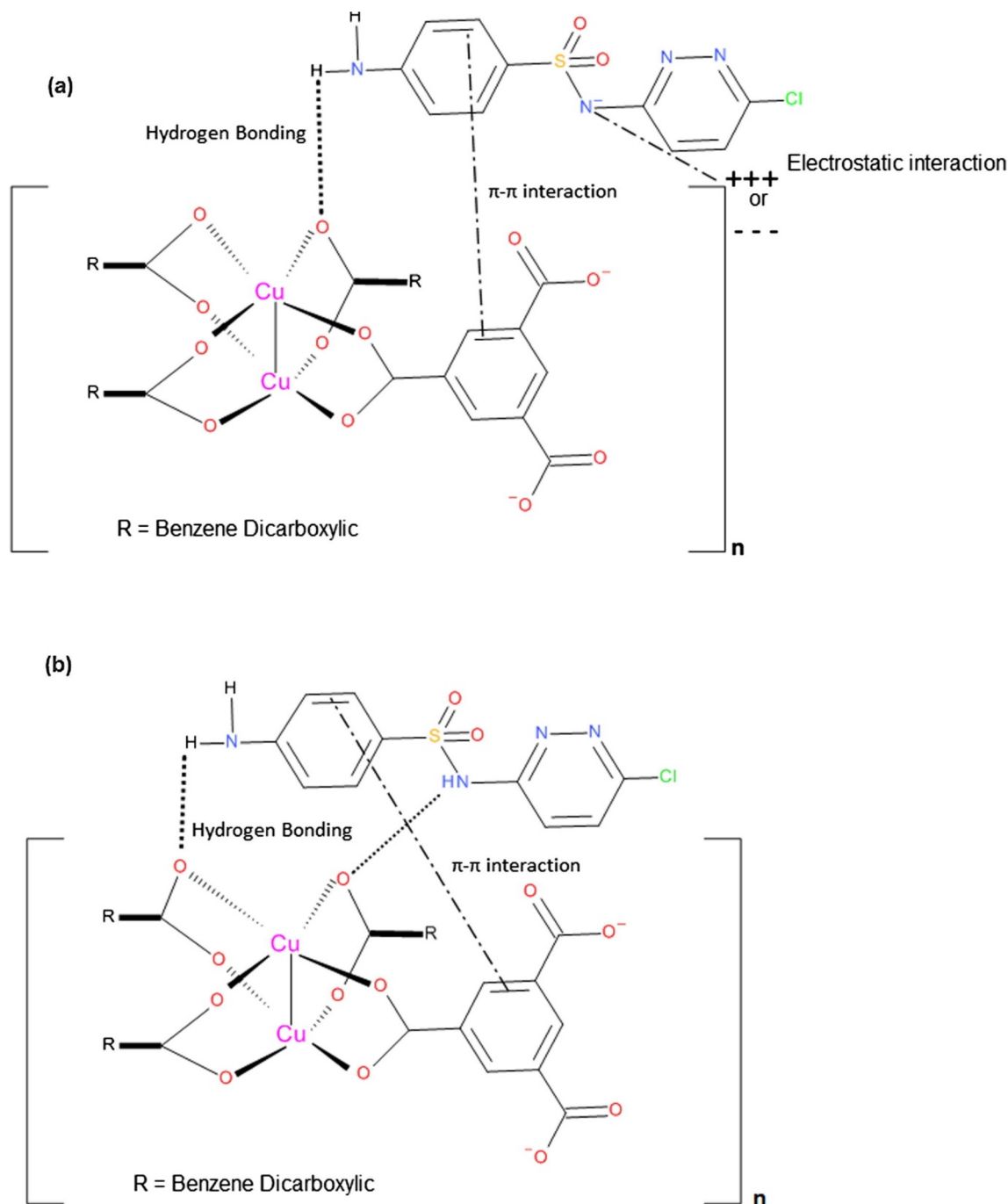
Fig. 5 Adsorption mechanism of SCP on HKUST-1, (a) H-bond formed with H of NH$_2$ from SCP and oxygen of HKUST-1 clusters, (b) H-bond between Cu–O–Cu and H of amide group is indicating the removal of SCP in its neutral form (adapted from ref. 103 with permission from Elsevier, copyright 2016).

Recent studies have reported that many MOFs, especially those with weak metal–ligand bonds, suffer from poor aqueous and thermal stability, which restricts their long-term use in water treatment.[104] Additionally, metal ion leaching from MOFs—particularly those based on transition metals such as Cu, Zn, and Fe—poses risks to environmental safety and downstream processes.[105] The potential toxicity of uncoordinated or degraded organic linkers, such as imidazolates and terephthalates, is also an emerging concern, especially under variable pH and oxidizing conditions.[106] We have incorporated these findings into the discussion to present a more nuanced and realistic evaluation of MOFs' applicability in pharmaceutical wastewater treatment.

5.3 Graphene and graphene-based materials for pharmaceutical wastewater treatment

Numerous sorbent materials have undergone thorough investigation for the elimination of heavy metal ions, which are
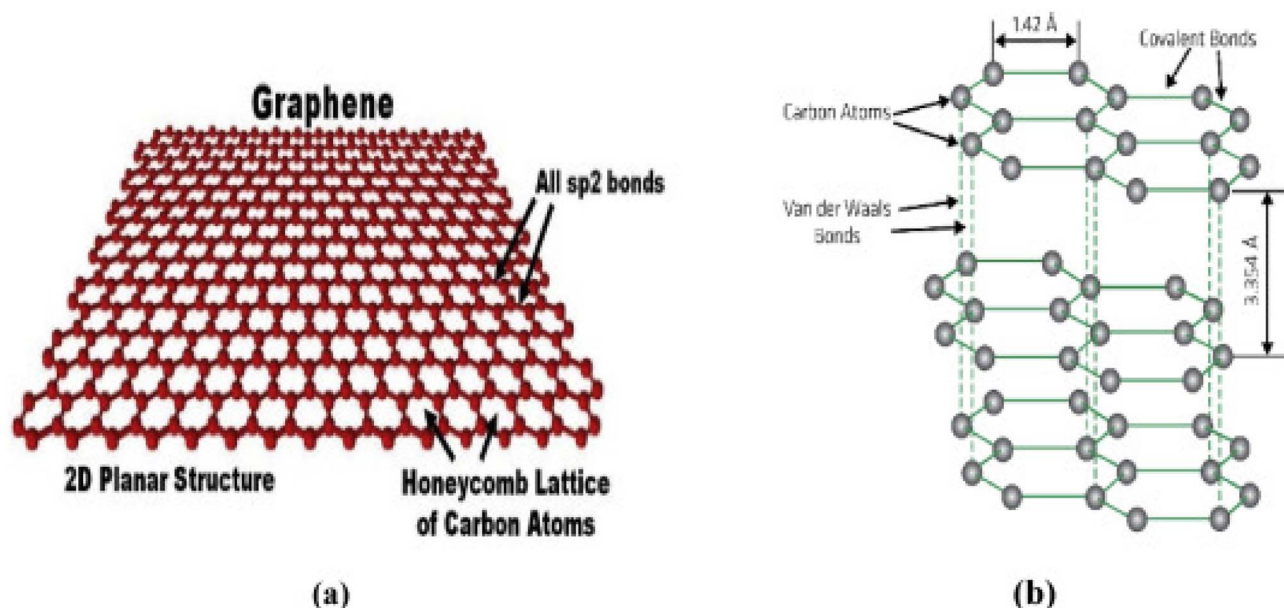
Fig. 6 (a) The sp^2 hybridization arrangement of carbon atoms, which are closely packed together in a honeycomb lattice formation. (b) The atomic structure of graphene, emphasizing the individual carbon atoms and their connections within the lattice (adapted from ref. 109 with permission from Elsevier, copyright 2020).

known to have either low sorption capacities or efficiencies. Graphene and its derivatives have recently gained popularity in wastewater treatment due to their exceptional thermal, optical, chemical, and mechanical properties, including a high surface area, excellent thermal conductivity, and high optical transmittance, among others. Graphene-based materials, including graphene oxide (GO) and reduced graphene oxide (rGO), have the potential to be modified with diverse functional groups, thereby augmenting their adsorption characteristics. It is reported that the adsorption mechanism of organic pollutants on graphene depends upon the π-electron system of the organic molecules and the π-electrons associated with the aromatic ring of graphene.

Graphene is a two-dimensional arrangement of carbon atoms organized in a hexagonal lattice structure, constituting a singular layer.[107] Fig. 6 shows the two-dimensional (2D) structure resulting from sp^2 hybridization of its carbon atoms arranged in a honeycomb framework.[108] The excellent dispersion properties of graphene are due to the weak van der Waals forces that bind the layers (bond length 0.142 nm) together.

The increasing interest in graphene originates from its remarkable physicochemical attributes, including its elevated specific surface area (a theoretical surface area of 2630 m^2 g^{-1}),[110] exceptional electrical and thermal conductivity,[111] chemical structure, and mechanical strength. Graphene acts as a rapid adsorbent for diverse contaminants thanks to its extensive, delocalized π-electron system, enabling robust interactions with other pollutants. Saravanan et al. provided an in-depth analysis of the applications of materials derived from graphene in wastewater treatment as adsorbents, electrodes, and photocatalysts to efficiently remove harmful pharmaceutical pollutants, heavy metals, dyes, and other contaminants, as shown in Fig. 7.[112]

The application of graphene-based materials as photocatalysts for removing decomposing organic contaminants from pharmaceutical effluent has been reported.[113] Graphene can enable the production of reactive oxygen species when paired with appropriate photocatalytic substances, such as metal oxides or semiconductors, and subjected to light irradiation.[114] These reactive species can facilitate the degradation of organic molecules into less detrimental chemicals via oxidation mechanisms. Jauris et al. investigated the adsorption behavior of sodium diclofenac (s-DCF) on several carbon-based materials, including pristine graphene, graphene with a vacancy, reduced graphene oxide (rGO), and functionalized graphene nanoribbons.[115] The primary objective of this research was to gain insights into the underlying process of s-DCF adsorption on the carbon lattice. The computer simulations demonstrated that the interactions between pristine graphene and s-DCF can be attributed to a physical adsorption mechanism. However, in the case of pristine graphene and graphene with a single vacancy, the outcomes indicated the presence of π–π interactions.

5.4 Metal oxide nanoparticles as adsorbents

The remarkable characteristics of nanoparticles, including their large surface-to-volume ratio, novel optical properties, and the ability to achieve any desired shape, have garnered considerable interest. Activated carbon-based sorbents have been extensively researched for their effectiveness in wastewater treatment. However, the challenge lies in separating and regenerating these sorbents due to their small size. To address this issue, magnetically active sorbents have been proposed, e.g., Fe$_2$O$_3$, ZnO, ZnO–MgO, Al$_2$O$_3$, TiO$_2$, CuO, MnO$_2$, and related conjugate sorbents.[116] The sorbents involve embedding oxides onto
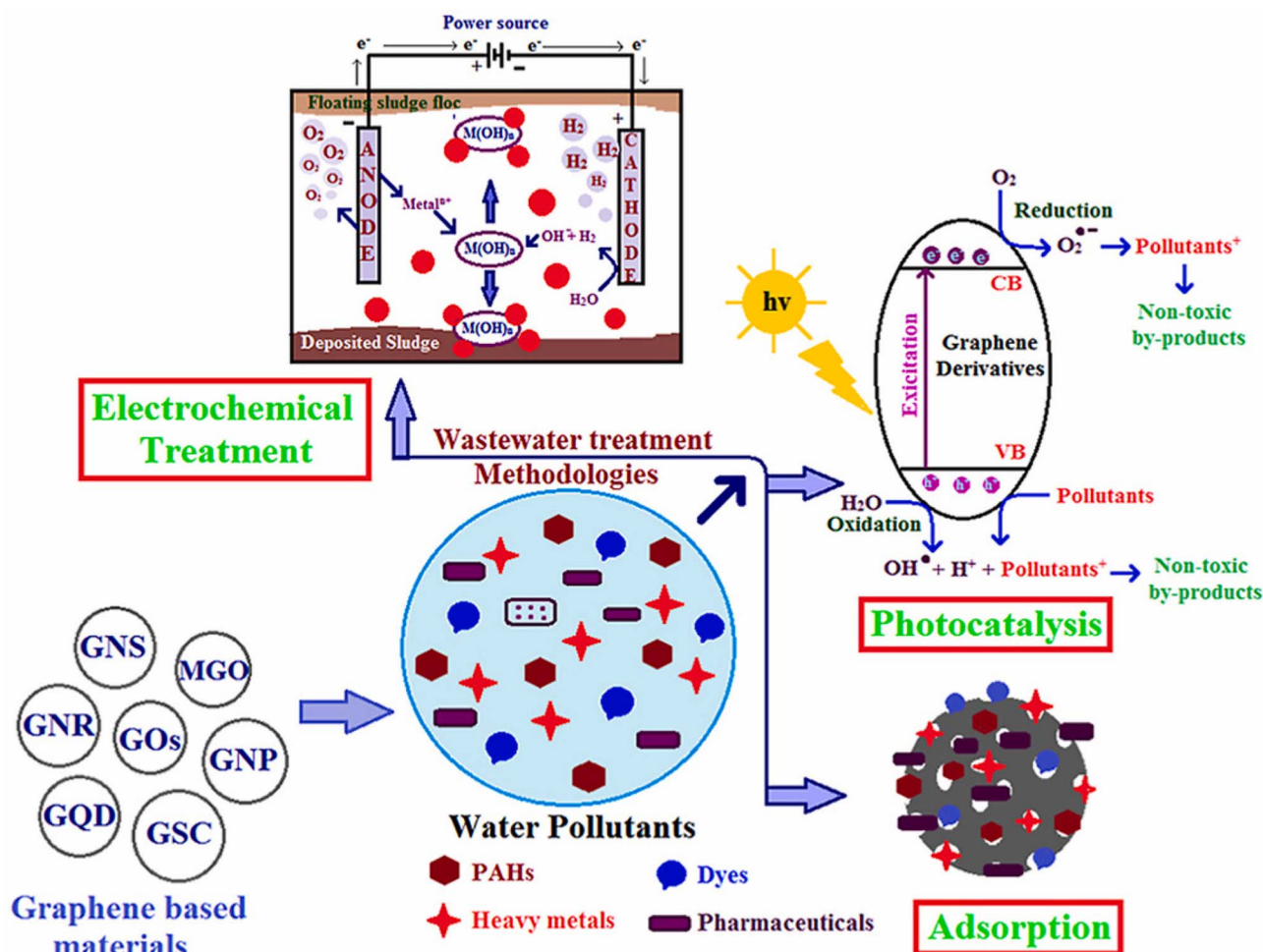
Fig. 7 A schematic representation of possible mechanisms for water pollutant removal by graphene adsorbents, photocatalysts, and electrodes (adapted from ref. 112 with permission from Elsevier, copyright 2022).

a carrier that prevents oxide aggregation. Nanoparticle techniques have proven vastly superior to conventional sorbents in pharmaceutical effluent treatment. There is an urgent need for research into the complexities of nanomaterials for pharmaceutical wastewater treatment, as several mechanisms are involved in pharmaceutical drug removal from wastewater.

Iron-based nanoparticles have been extensively studied in various forms, including doped, composite, and spinel oxides. Various chemical methods have been reported for synthesizing pristine/doped/composite iron oxide nanoparticles, including co-precipitation, sol–gel, thermal decomposition, hydrothermal, and polyol methods. Other physical methods include solid-state ball milling, gas phase deposition, and pulsed-laser ablation. Hematite (α-Fe$_2$O$_3$), among various iron oxide polymorphs, has garnered significant attention due to its exceptional resistance to corrosion, non-toxic nature, high stability in atmospheric conditions, and environmentally friendly properties. The particle size, shape, and composition of chemically synthesized iron nanoparticles (NPs) are influenced by various factors, including the precursor salt type, Fe(II) to Fe(III) ratio, pH, and ionic strength. In a study by Ali *et al.*, five types of

adsorptive removal mechanisms were outlined for iron-based nanoparticles.[117] These mechanisms include the electrostatic interaction between pollutants and magnetic nanomaterials, facilitated by diverse biomolecules present on the surfaces of magnetic nanoparticles. Chemical diffusion occurs between the adsorbent and adsorbate, while surface precipitation, redox reactions, and ion exchange are also significant mechanisms. Hydroxyl (OH) functional groups play a crucial role in the ion exchange process. The tendency of different groups of antibiotics to dissociate into cations, zwitterions, and anions at varying pH levels cannot make their mechanism of adsorption a stereotype. Hence, in addition to experimental techniques, density functional theory calculations can provide crucial insights into the mechanism of removing contaminants.

5.5 Sustainable materials as adsorbents

Solid materials used as adsorbents can take a broad range of chemical forms and different geometrical surface structures. There are also basic types of adsorbents, including carbon adsorbents, mineral adsorbents, and others. The adsorbent can

Table 4 Adsorption capacities, specific surface areas, adsorption conditions, adsorption kinetics and isotherms, and potential mechanisms for the removal of pharmaceuticals from wastewater

Adsorbent	Synthesis techniques	Characterization techniques	Adsorbate	Surface area (m² g⁻¹)	Experimental conditions	Maximum experimental adsorption capacity (mg g⁻¹)	Adsorption capacity per unit surface area (mg m⁻²)	Adsorption isotherm	Adsorption kinetics	Thermodynamic parameters (ΔG kJ mol⁻¹, ΔH kJ mol⁻¹, and ΔS J mol⁻¹ K⁻¹)	Key insights	Reference
Zeolite (ZPC800)	Microwave-assisted solvothermal method, pyrolysis temperature 800 °C	Surface: BET	Tetracycline	268	pH 6, initial adsorbent dosage = 100 mg L⁻¹, contact time = 300 min	317.50	1.18	Temkin	Elovich	—	Heterogeneous surface adsorption, non-uniform surface energy adsorption	150
	Microwave-assisted solvothermal method, pyrolysis temperature 800 °C	Structural morphology: SEM, adsorption quantification: UV-vis Others: XRD, FTIR	Ciprofloxacin		pH 8, initial adsorbent dosage = 40 mg L⁻¹, contact time = 350 min	270.67	0.99	Temkin	Pseudo-second-order	—	Chemisorption on heterogeneous surface	151
Zeolite (HSZ-690HOA zeolite)	Commercial high silica zeolite mordenite, calcination temperature 800 °C	Surface: BET Adsorption quantification: HPLC-UV, HPLC-MS Others: NMR, TGA	Sulfachloropyridazine	453	At 25 °C and 65 °C, 4 h contact time	151	0.33	N/A	N/A	—	Hydrogen bonding	151
Zeolite (faujasite zeolite Y)	"Y" type faujasite zeolite powder with a 200 SiO₂/Al₂O₃ (mol mol⁻¹) ratio	Surface: BET others: TGA, XRD	Sulfonamide	852	At 25 °C and 65 °C, pH 5.8, 24 h contact time	280	0.33	N/A	N/A	—	N/A	94
Zeolite (ZIF-8)	Sonochemical synthesis, activated by heating under vacuum at 80 °C	Surface: BET Structural morphology: SEM Adsorption quantification: HPLC-UV, HPLC-FD Others: XRD, FTIR	Ofloxacin		At pH 7.7, 10 mg adsorbent L⁻¹	95 ± 10	0.31	Langmuir	Pseudo-second-order	—	Chemisorption	152
Zeolite (zeolite Y)	Sol–gel method, calcination temperature 500 °C	Surface: BET Structural morphology: SEM Others: XRF, XRD, FTIR	Tetracycline	657.44	At 30 °C, pH 6.7	201.77		Langmuir	Pseudo-second-order	—	Chemisorption	153

Table 4 (Contd.)

Adsorbent	Synthesis techniques	Characterization techniques	Adsorbate	Surface area ($m^2\ g^{-1}$)	Experimental conditions	Maximum experimental adsorption capacity ($mg\ g^{-1}$)	Adsorption capacity per unit surface area ($mg\ m^{-2}$)	Adsorption isotherm	Adsorption kinetics	Thermodynamic parameters (ΔG kJ mol^{-1}, ΔH kJ mol^{-1}, and ΔS J mol^{-1} K^{-1})	Key insights	Reference
Zeolite (PZ-NZVI)	One-pot method	Surface: BET Structural morphology: SEM, EDS Others: XPS, XRD, FTIR, TGA	Norfloxacin, ofloxacin	26.48	At pH 4–10	54.67 mg g^{-1} for norfloxacin and 48.88 mg g^{-1} for ofloxacin	2.06 mg m^{-2} for norfloxacin and 1.85 mg m^{-2} for ofloxacin	Langmuir	Pseudo-second-order	−27.2, −6.98, 70.3 for NOR −26.63, −17.97, 30.3 for OFL	Electrostatic, hydrophobic interaction and complexation, spontaneous and exothermic adsorption	95
Zeolite (magnetic GO/ZIF-8/AlOOH-NC)	Combining the solvothermal and solid-state dispersion method	Surface: BET Structural morphology: FE-SEM, EDS Others: AFM, XRD, FTIR, TGA	Diclofenac sodium	777	At 30 °C, pH 7.5, equilibrium time 50 min	2594	3.33	Langmuir	Pseudo-second-order	—	H-bonding, electrostatic attraction, n-pi interaction, π–π interaction, physical interaction	96
Zeolite (CTAB-ZIF-67)	—	Surface: BET Structural morphology: FE-SEM, EDS Others: Zeta potential, XRD, FTIR, TGA	Diclofenac sodium	709–1103	At pH 5–10, 90 min equilibrium time	60.60	0.08	Langmuir	Pseudo-second-order	−29.53, 40, 240	Electrostatic attraction, spontaneous, and endothermic	154
Zeolite (ZCPC)	Raw clinoptilolite-rich zeolitic tuff from Zlatokop deposit	Surface: BET Others: Zeta potential, FTIR, TGA	Diclofenac sodium		At pH 7.4, 60 min equilibrium time	160		Langmuir	N/A	—	N/A	155
Zeolite (MoS$_2$@zeolite-5)	Combining the ultrasonic and hydrothermal method	Surface: BET Structural morphology: SEM, EDS, HR-TEM Others: XPS, XRD, FTIR	Tetracycline	15.82	At 35 °C, at pH 4	396.70	25.08	Langmuir	Pseudo-second-order	−0.806, 66.17, 224.98	Chelation, electrostatic action, π–π action, and H-bonding	97
Zeolite (MNCZ)	—	Surface: BET Adsorption quantification: LC-MS/MS	Diclofenac-Na, naproxen, gemfibrozil and ibuprofen		At pH 2	Removal efficiency > 99%		Freundlich	Pseudo-second-order	—	Chemi-sorption	98

Table 4 (Contd.)

Adsorbent	Synthesis techniques	Characterization techniques	Adsorbate	Surface area ($m^2 g^{-1}$)	Experimental conditions	Maximum experimental adsorption capacity ($mg\ g^{-1}$)	Adsorption capacity per unit surface area ($mg\ m^{-2}$)	Adsorption isotherm	Adsorption kinetics	Thermodynamic parameters (ΔG kJ mol^{-1}, ΔH kJ mol^{-1}, and $\Delta SJ\ mol^{-1}\ K^{-1}$)	Key insights	Reference
Zeolite (modified zeolite)	Modified by equilibrating RZ and HDTMA solutions	Surface: BET, adsorption quantification: HPLC; Structural morphology: SEM; Others: Contact angle, FTIR, zeta potential	Estrone and 17β-estradiol		At pH 5–7, low temperature	8.29 mg g^{-1} for estrone and 7.09 mg g^{-1} 17β-estradiol		Langmuir	Pseudo-second-order	—	Distribution effects and surface adsorption	99
Zeolite (FeO-NCP)	Dry milling method	Surface: BET Adsorption quantification: UV-vis; Structural morphology: SEM, TEM; Others: AAS, FTIR, XRD, TOC	Tetracycline		At pH 5	>50% degradation		N/A	N/A	—	N/A	156
Zeolite (TiO₂/zeolite)	Acid-activated and acid-alkali-activated zeolites	Surface: BET Adsorption quantification: HPLC, LC-MS; Structural morphology: SEM, EDS; Others: XRD	Amoxicillin		240 min irradiation time	>99% removal efficiency		N/A	N/A	—	N/A	157
MOF (amino-functionalized MIL-88B(Fe)-based porous carbon)	Microwave-assisted solvothermal method	Surface: BET Structural morphology: SEM; Others: XRD, XPS	Ciprofloxacin	215.1	At 700 °C pyrolysis, pH 6, adsorbent 0.1 g L^{-1}, contact time 240 min	102.5	0.48	Freundlich	Pseudo-second-order	—	Chemisorption	158
MOF (MPC800)	Solvothermal method, pyrolysis temperature 800 °C	Surface: BET Structural morphology: SEM, TEM; Others: XRD, FTIR, RAMAN	Ciprofloxacin	199	At 800 °C pyrolysis, pH 4, adsorbent dosage 0.1 g L^{-1}, ionic strength 0.4 mol L^{-1}	90.9	0.46	Langmuir	Pseudo-second-order	—	Chemisorption, electrostatic attraction	159

Table 4 (Contd.)

Adsorbent	Synthesis techniques	Characterization techniques	Surface area ($m^2 g^{-1}$)	Adsorbate	Experimental conditions	Maximum experimental adsorption capacity ($mg\ g^{-1}$)	Adsorption capacity per unit surface area ($mg\ m^{-2}$)	Adsorption isotherm	Adsorption kinetics	Thermodynamic parameters (ΔG kJ mol^{-1}, ΔH kJ mol^{-1}, and ΔS J mol^{-1} K^{-1})	Key insights	Reference
MOF (Cr-based MOF (MIL-101))	Hydrothermal method	Surface: BET Others: XRD	3014	Naproxen, clofibric acid	At 25 °C, pH 4.5, contact time 12 h, 100 g adsorbent L^{-1}	132 mg g^{-1} for naproxen, 244 mg g^{-1} for clofibric acid	0.04 mg m^{-2} for naproxen, 0.08 mg m^{-2} for clofibric acid	Langmuir	Pseudo-second-order	—	Electrostatic interaction	100
MOF (acidic Cr-based MOF (AMSA-MIL-101))	Hydrothermal method	Surface: BET Others: XRD, FTIR, elemental analyzer	2322	Naproxen, clofibric acid	At 25 °C, pH 4.5, 100 g adsorbent L^{-1}	93 mg g^{-1} for naproxen, 105 mg g^{-1} for clofibric acid	0.04 mg m^{-2} for naproxen, 0.05 mg m^{-2} for clofibric acid	Langmuir	Pseudo-second-order	—	Acid-base interaction	160
MOF (basic Cr-based MOF (ED-MIL-101))	Hydrothermal method	Surface: BET Others: XRD, FTIR, elemental analyzer	2555	Naproxen, clofibric acid	At 25 °C, pH 4.5, 100 g adsorbent L^{-1}	154 mg g^{-1} for naproxen, 347 mg g^{-1} for clofibric acid	0.06 mg m^{-2} for naproxen, 0.14 mg m^{-2} for clofibric acid	Langmuir	Pseudo-second-order	—	Acid-base interaction	160
MOF (al-based MOF[MIL-53(Al)])	Hydrothermal method	Surface: BET Structural morphology: STEM-HAADF, TEM Others: XRD, XPS, FTIR	1401	Nitroimidazole	At 30 °C, pH 6.4, 1 g adsorbent L^{-1}	467.3	0.33	Langmuir	Pseudo-second-order	—	Van der Waals interaction	161
MOF (MIL-101-urea)	Hydrothermal method	Surface: BET Others: XRD, elemental analyzer, FTIR	1970	Nitroimidazole	At 25 °C, 12 h contact time, pH 6.3	185 mg L^{-1} for DMZ, 188 mg g^{-1} for MNZ	0.09 mg m^{-2} for DMZ, 0.1 mg m^{-2} for MNZ	Langmuir	N/A	—	H-bond	162
MOF (methanol-activated Cu-based MOF (HKUST-1))	Hydrothermal method, activated by methanol	Surface: BET Structural morphology: SEM Others: XRD, TGA, FTIR	1700	Sulfachloro-pyridazine	At 25 °C, pH = 7.5, 0.1 g adsorbent L^{-1}	384	0.22	Langmuir	Pseudo-second-order	−28.8, 4, 110.3	π–π stacking, H-bonding, electrostatic interaction, spontaneous, and endothermic adsorption	102
MOF (chloroform-activated Zr-based MOF (UiO-66))	Modified solvothermal method	Surface: BET Structural morphology: SEM Others: XRD, TGA, FTIR	1155	Sulfachloro-pyridazine	At 25 °C, pH 5.5, 0.1 g adsorbent L^{-1}	417	0.36	Langmuir	Pseudo-second-order	−30.4, −60.6, −100.9	Hydrophobicity, π–π interaction, electrostatic interaction, spontaneous, and endothermic adsorption	163

Table 4 (Contd.)

Adsorbent	Synthesis techniques	Characterization techniques	Adsorbate	Surface area (m² g⁻¹)	Experimental conditions	Maximum experimental adsorption capacity (mg g⁻¹)	Adsorption capacity per unit surface area (mg m⁻²)	Adsorption isotherm	Adsorption kinetics	Thermodynamic parameters (ΔG kJ mol⁻¹, ΔH kJ mol⁻¹, and ΔS J mol⁻¹ K⁻¹)	Key insights	Reference
MOF (CFC/UiO-66-NH₂/AgI)	Microwave-assisted hydrothermal method	Surface: BET Adsorption quantification: UV-vis, LC-MS Structural morphology: FE-SEM, TEM, HR-TEM Others: XRD, XPS	Levofloxacin, ciprofloxacin	730.8	At 4.5–8.5 pH, 10 mg adsorbent L⁻¹	Degrade 84.5% levofloxacin, 79.6% ciprofloxacin		N/A	N/A	—	N/A	164
MOF (copper meso-tetra (4-carboxyphenyl) porphine MOFs)	Modified solvothermal method	Surface: BET Adsorption quantification: UV-vis Structural morphology: FE-SEM, TEM, AFM Others: XRD, FTIR, XPS, UPS, zeta potential	Oxytocin, tetracycline	342.72	0.2 g adsorbent L⁻¹	130 mg g⁻¹ for oxytocin, 150 mg g⁻¹ for tetracycline	0.38 mg m⁻² for oxytocin, 0.44 mg m⁻² for tetracycline	Langmuir	Pseudo-second-order	—	Chemisorption	165
MOF (MIL-101)	Solvothermal method	Surface: BET Adsorption quantification: UV-vis Structural morphology: SEM, EDS Others: XRD, FTIR, XPS, zeta potential	Tetracycline hydrochloride	180.41	pH 10.2, 0.15 g adsorbent L⁻¹, 10 mL L⁻¹ H₂O₂	82.52% tetracycline hydrochloride removal efficiency		N/A	Pseudo-second-order	—	Photo–Fenton reaction	166
MOF (UiO-66-NH₂)	Modified hydrothermal method	Surface: BET Structural morphology: SEM, TEM Others: XRD, FTIR, XPS, TGA	Norfloxacin	713.20	At 0.10 g adsorbent L⁻¹, pH 8	222.5	0.31	Langmuir	Pseudo-second-order	—	Electrostatic, π–π and hydrophobic interaction	167
MOF (Zn₃(BTC)₂)	Synthesis in a purely aqueous system	Surface: BET Structural morphology: SEM Others: XRD, FTIR	Ofloxacin		At pH 7.7, 10 mg adsorbent L⁻¹	25.3 ± 0.8		Sigmoidal	Sigmoidal	—	N/A	152

Table 4 (*Contd.*)

Adsorbent	Synthesis techniques	Characterization techniques	Adsorbate	Surface area ($m^2 g^{-1}$)	Experimental conditions	Maximum experimental adsorption capacity ($mg\ g^{-1}$)	Adsorption capacity per unit surface area ($mg\ m^{-2}$)	Adsorption isotherm	Adsorption kinetics	Thermodynamic parameters (ΔG kJ mol^{-1}, ΔH kJ mol^{-1}, and ΔS J mol^{-1} K^{-1})	Key insights	Reference
MOF (Zr/Fe-MOF/GO)	Hydrothermal method	Surface: BET Structural morphology: SEM Others: FTIR, TGA	Tetracycline hydrochloride		At pH 6.7, 20 mg adsorbent L^{-1}	156		Freundlich	Pseudo-first order	—	Chemisorption	168
MOF (alginate-graphene-ZIF67)	Modified Hummers' method	Surface: BET Structural morphology: SEM Others: XRD, FTIR, XPS	Tetracycline	138.62	At 30 °C, pH 6	456.62	3.29	Freundlich	Pseudo-second-order	—	π–π interaction and cation-pi bond	169
MOF (UiO-66-(COOH)$_2$/GO)	Modified hydrothermal method	Surface: BET Structural morphology: SEM Others: XRD, FTIR, XPS, TGA	Tetracycline hydrochloride	369.60	At universal pH, 0.50 g adsorbent L^{-1}	164.91	0.45	Langmuir	Pseudo-second-order	—	π–π interaction, chemical coordination, and weak electrostatic interaction	170
MOF (UiO-66-NH-BT@g-C$_3$N$_4$)	Hydrothermal method	Surface: BET Structural morphology: SEM Others: XRD, XPS	Sulfamethoxazole		At pH 7, 25 mg PS dosage	97.6% sulfamethoxazole removal efficiency		N/A	N/A	—	N/A	171
Graphene (graphite rods (15 cm in length and 1 cm in diameter))	Electrochemical exfoliation method	Surface: BET Structural morphology: TEM	Di-n-butyl phthalate (DnBP), di-(2-ethylhexyl) phthalate (DEHP), acetaminophen (ACE), caffeine, cephalexin (CLX), and sulfamethoxazole (SMX)		At 0.10 g adsorbent L^{-1} and adsorption time of 12 h	27.03, 39.22, 18.28, 22.73, 23.47, 17.42 respectively		Langmuir	Pseudo-second-order	—	Chemisorption	172

Table 4 (*Contd.*)

Adsorbent	Synthesis techniques	Characterization techniques	Adsorbate	Surface area (m² g⁻¹)	Experimental conditions	Maximum experimental adsorption capacity (mg g⁻¹)	Adsorption capacity per unit surface area (mg m⁻²)	Adsorption isotherm	Adsorption kinetics	Thermodynamic parameters (ΔG kJ mol⁻¹, ΔH kJ mol⁻¹, and ΔS J mol⁻¹ K⁻¹)	Key insights	Reference
Graphene (NiZrAl-layered double hydroxide-graphene oxide-chitosan)	Hydrothermal method	Surface: BET; Structural morphology: SEM, TEM, EDX; Others: XRD, RAMAN, pHZPC	Nalidixic acid	128.30	At pH 8, 10 mg of adsorbent dosage	277.79	2.17	Temkin and Freundlich	Pseudo-second-order	—	Chemisorption	173
Graphene (graphene oxide (GO))	Modified Hummers' method	Surface: BET; Adsorption quantification: UV-vis, structural morphology: AFM; Others: XRD, FTIR, RAMAN	Tetracycline		At pH 3.6, 0.181 mg of adsorbent mL⁻¹	313		Langmuir and Temkin	Pseudo-second-order	—	Electrostatic interaction, π–π interaction, and cation–π bonding	174
Graphene (graphene nanoparticles (GNP))	Hydrothermal method	Surface: BET; Adsorption quantification: HPLC-UV; Structural morphology: TEM; Others: XRD	Caffeine, acetaminophen, aspirin	635	At pH 8, 1 mg of adsorbent mL⁻¹	18.76, 19.72, 13.02	0.03,0.031,0.02	N/A	Pseudo-second-order	—	N/A	175
Graphene (reduced graphene oxide (rGO))	Hydrothermal method	Surface: BET; Structural morphology: SEM, TEM, EDX; Others: XRD, FTIR, TGA	Ciprofloxacin, norfloxacin		At pH 6.2, 2 mg of adsorbent dosage	18.22–22.20		Langmuir and Temkin	Pseudo-second-order	—	Electrostatic interaction, π–π interaction, and cation–π bonding	176
Graphene (GO nanoparticles)	Hummers' method	Surface: BET; Structural morphology: SEM, FE-SEM, TEM, EDX; Others: XRD, FTIR, RAMAN, zeta potential, DLS, solid-state NMR	Metformin	187.2	At pH 6.26, (50–150) mg of adsorbent dosage	122.61	0.66	Freundlich	Pseudo-first order	−135.76, −2.15, 4.47	Chemisorption, spontaneous, and endothermic adsorption process	177

Table 4 (*Contd.*)

Adsorbent	Synthesis techniques	Characterization techniques	Adsorbate	Surface area (m² g⁻¹)	Experimental conditions	Maximum experimental adsorption capacity (mg g⁻¹)	Adsorption capacity per unit surface area (mg m⁻²)	Adsorption isotherm	Adsorption kinetics	Thermodynamic parameters (ΔG kJ mol⁻¹, ΔH kJ mol⁻¹, and ΔS J mol⁻¹ K⁻¹)	Key insights	Reference
Graphene (rGO)	Hydrothermal method	Surface: BET; Structural morphology: SEM, AFM; Others: FTIR, RAMAN, TGA	Sodium diclofenac drug (s-DCF)		At pH 8–10, 30 mg of adsorbent dosage	59.67		Liu	General order	—	π–π interaction	115
Graphene (graphene oxide composite reinforced with carboxymethyl cellulose)	Improved Hummers' method	Surface: BET; Structural morphology: FE-SEM, EDX; Others: FTIR, PZC, TGA	Amitriptyline (tricyclic antidepressant drug)		At pH 2–11, (2.5–40) mg of adsorbent dosage	737.4		Langmuir	Pseudo-second-order	—	Chemisorption and physisorption	178
Graphene (carbon xerogel/graphene hybrid)	Hydrothermal method	Surface: BET; Structural morphology: SEM; Others: XPS, RAMAN	Metronidazole (MNZ)	(648–816)	At pH 5 and 298 K	110–166	0.17–20	Freundlich–Langmuir	N/A	—	π–π and electrostatic interactions and hydrogen bonding	179
Biochar (hazelnut shell-based magnetic biochar)	Pyrolysis method	Surface: BET; Structural morphology: SEM, EDX; Others: FTIR, XRD, TGA	Penicillin-G		At 40 °C, pH = 2, 1000 ppm Pen-G concentration, and 0.175 g of catalyst per 100 g of solution	479		Langmuir	Pseudo-second-order	—	Chemisorption	120
Biochar (iron-loaded sludge biochar)	Pyrolysis method	Surface: BET; Structural morphology: SEM, EDS, TEM; Others: FTIR, XRD, XRF, XPS	Tetracycline (TC)	82.78 m² g⁻¹	pH 2, contact time = 48 h, biochar dosage = 0.6 g L⁻¹, initial TC concentration = 60 mg L⁻¹	104.86	1.27	Langmuir	Pseudo-second-order	—	π–π interaction, hydrogen bonds, complexation, and electrostatic interaction	121
Biochar (sewage sludge-derived biochar)	Pyrolysis method	Surface: BET	Diclofenac (DCF)	69.7–104.1	At 500 °C, pH 3–6, contact time = 3 h, initial (DCF) concentration = 10–100 mg L⁻¹	92.7		Dubinin–Radushkevich	Pseudo-second-order	—	π-stacking interactions	123
Biochar (maple leaf-derived biochar)	Pyrolysis method	Surface: BET; Structural morphology: SEM; Others: FTIR, XRD, XPS, TGA, ICP-OES, pHPZC	Tetracycline (TC)	191.1	pH 6–9, contact time = 5 days, biosorbent dosage = 0.01 g L⁻¹, initial TC concentration = 100 mg L⁻¹	407.3	2.13	Freundlich	Pseudo-second-order	—	Metal complexation, H-bonding, and hydrophobic interactions	124

Table 4 (*Contd.*)

Adsorbent	Synthesis techniques	Characterization techniques	Adsorbate	Surface area ($m^2\ g^{-1}$)	Experimental conditions	Maximum experimental adsorption capacity ($mg\ g^{-1}$)	Adsorption capacity per unit surface area ($mg\ m^{-2}$)	Adsorption isotherm	Adsorption kinetics	Thermodynamic parameters (ΔG kJ mol^{-1}, ΔH kJ mol^{-1}, and ΔS J mol^{-1} K^{-1})	Key insights	Reference
Biochar (algal-based (spirulina species) biochar)	Pyrolysis method	Surface: BET Structural morphology: SEM Others: FTIR, XRD, XPS, TGA, ICP-OES, pHPZC, elemental analyzer	Tetracycline (TC)	1.55 (specific surface area)	At 550 °C, pH 6, contact time = 48 h, biochar dosage = 0.05 g L^{-1}, initial TC concentration = 100 mg L^{-1}	132.8		Langmuir	Pseudo-first order	—	Hydrophobic, π–π interactions, functional groups, and metal complexation	125
Biochar (walnut shell biochar)	Pyrolysis method	Surface: BET Adsorption quantification: HPLC-UV Structural morphology: SEM Others: FTIR, XRD, XPS, RAMAN, elemental analyzer	Sulfadiazine	32	At 25 °C, pH 1–10, contact time = 48 h, biochar dosage = 0.02 g L^{-1}, initial sulfadiazine concentration = 20 mg L^{-1}	32		Freundlich	Elovich	—	π–π EDA interaction, hydrogen bond, electrostatic interaction, Lewis's acid–base interaction, and hydrophobic interaction	126
Biochar (sugarcane bagasse-derived biochar)	Pyrolysis method	Surface: BET Structural morphology: SEM, EDS Others: FTIR, XRD, pHPZC	Sulfamethoxazole	1099	At 303 K, pH 2–10, contact time = 80–90 min, biochar dosage = 0.05 g L^{-1}, initial sulfadiazine concentration = 100 mg L^{-1}	400	0.37	Freundlich	Elovich	—	π–π interaction and hydrogen bonding	127
Biochar (peanut shell-derived biochar)	Pyrolysis method	Surface: BET Structural morphology: SEM Others: FTIR, XRD, pHPZC, RAMAN	Naproxen	596	At 25 °C, pH 7, contact time = 48 h, biochar dosage = 0.5 g L^{-1}, initial naproxen concentration = 1000 mg L^{-1}	324		Langmuir	Pseudo-second-order	−20.3, −18.8, 4.47	Pore filling, π–π interaction, hydrogen bonding formations, n–π interaction, van der Waals force, and electrostatic attraction	129
Biochar (bamboo sawdust)	Pyrolysis method	Surface: BET Structural morphology: SEM Others: FTIR, XRD, RAMAN	Acetaminophen	1158.05	At 25 °C, pH 6.8, contact time = 120 min, biochar dosage = 0.5 g L^{-1}, initial acetaminophen concentration = 20 mg L^{-1}	192.43		Langmuir	Pseudo-second-order	—	Chemisorption	180

Table 4 (Contd.)

Adsorbent	Synthesis techniques	Characterization techniques	Adsorbate	Surface area ($m^2\ g^{-1}$)	Experimental conditions	Maximum experimental adsorption capacity ($mg\ g^{-1}$)	Adsorption capacity per unit surface area ($mg\ m^{-2}$)	Adsorption isotherm	Adsorption kinetics	Thermodynamic parameters (ΔG kJ mol⁻¹, ΔH kJ mol⁻¹, and ΔS J mol⁻¹ K⁻¹)	Key insights	Reference
Biochar (bamboo sawdust)	Pyrolysis method	Surface: BET, Structural morphology: SEM, Others: FTIR, XRD, RAMAN	Ciprofloxacin	1158.05	At 25 °C, pH 6.8, contact time = 120 min, biochar dosage = 0.5 g L⁻¹, initial ciprofloxacin concentration = 20 mg L⁻¹	70.95		Langmuir	Pseudo-second-order	—	Chemisorption	180
Biochar (corn-cob-derived biochar)	Pyrolysis method	Surface: BET, Structural morphology: SEM, Others: FTIR, XRD, RAMAN	Acetaminophen	1201.1	At 20–40 °C, pH 2–12, contact time = 0–350 min, biochar dosage = 1 g L⁻¹, initial acetaminophen concentration = 0–500 mg L⁻¹	332.08		Langmuir	Pseudo-second-order	−8.58, −44.39, −0.12	Hydrogen bonding formation and n–π interactions	181
Biochar (corn-cob-derived biochar)	Pyrolysis method	Surface: BET, Structural morphology: SEM, Others: FTIR, XRD, RAMAN	Amoxicillin	1201.1	At 20–40 °C, pH 2–12, contact time = 0–360 min, biochar dosage = 1 g L⁻¹, initial amoxicillin concentration = 0–500 mg L⁻¹	175.86		Freundlich	Pseudo-first order	−1.02, −4.68, −0.01	Hydrogen bonding formation and n–π interactions	181
Biochar (Prosopis juliflora)	Pyrolysis method	Surface: BET, Structural morphology: SEM, EDX, Others: FTIR, XRD, pHPZC, proximate analysis, TGA	Sulfamethoxazole	875.8	At 25–50 °C, pH 8, contact time = 120 min, biochar dosage = 1 g L⁻¹, initial sulfamethoxazole concentration = 50 mg L⁻¹	49.776		Langmuir	Pseudo-second-order	—	Chemisorption	182
Biochar (Prosopis juliflora)	Pyrolysis method	Surface: BET, Structural morphology: SEM, EDX, Others: FTIR, XRD, pHPZC, proximate analysis, TGA	Ciprofloxacin	875.8	At 25–50 °C, pH 5, contact time = 120 min, biochar dosage = 1 g L⁻¹, initial ciprofloxacin concentration = 50 mg L⁻¹	91.432		Langmuir	Pseudo-second-order	—	Chemisorption	182
Agricultural waste-based materials (coconut shell-derived activated carbon)	Pyrolysis method	Surface: BET, Adsorption quantification: UV-vis, Others: TGA, pHPZC	Levodopa	1175	At 25 °C, pH 6.2, contact time = 120 min, initial dosage = 0.1 g L⁻¹, initial levodopa concentration = 0.013 mg L⁻¹	285.3	0.24	Freundlich	N/A	—	Donor–acceptor mechanism	183

Table 4 (*Contd.*)

Adsorbent	Synthesis techniques	Characterization techniques	Adsorbate	Surface area (m² g⁻¹)	Experimental conditions	Maximum experimental adsorption capacity (mg g⁻¹)	Adsorption capacity per unit surface area (mg m⁻²)	Adsorption isotherm	Adsorption kinetics	Thermodynamic parameters (ΔG kJ mol⁻¹, ΔH kJ mol⁻¹, and ΔS J mol⁻¹ K⁻¹)	Key insights	Reference
Agricultural waste-based materials (carbon foam pellets derived from *Vallisneria natans*)	Ball milling, pyrolysis method, hydrothermal method	Surface: BET Structural morphology: SEM Others: FTIR, XRD, pHPZC, elemental analyzer, TGA	Metronidazole	922.56	At 30 °C, pH 9,0, contact time = 120 min, initial dosage = 6.0 g L⁻¹, initial metridazole concentration = 10 mg L⁻¹	64.23	0.069	Langmuir	Pseudo-first order	—	Hydrogen bonding, π–π interactions, and micropore filling	184
Agricultural waste-based materials (grapestalk-derived activated carbon)	Knife milling, hydrothermal method	Surface: BET Others: pHPZC	Caffeine	1099.86	At 30 °C, pH 4, contact time = 30 min, initial dosage = 15.0 g L⁻¹, initial caffeine concentration = 5–35 mg L⁻¹	916.7	0.83	Sips	N/A	—	N/A	133
Agricultural waste-based materials (iron(III)-loaded bamboo cellulose nanofibers)	Mechanical shearing method, freeze-dryer	Surface: BET Structural morphology: SEM, EDS Others: FTIR, XRD, pHPZC, XPS, TGA	Tetracycline (TC)	171	At 25 °C, pH 7, contact time = 30 min, initial adsorbent dosage = 0.5 mg L⁻¹, initial caffeine concentration = 5–10 mg L⁻¹	294.12	1.72	Langmuir	Pseudo-second-order	—	Surface complexation, hydrogen bonding, electrostatic interaction, and van der Waals force	185
Agricultural waste-based materials (iron(III)-loaded bamboo cellulose nanofibers)	Mechanical shearing method, freeze-dryer	Surface: BET Structural morphology: SEM, EDS Others: FTIR, XRD, pHPZC, XPS, TGA	Chlortetracycline	171	At 25 °C, pH 7, contact time = 30 min, initial adsorbent dosage = 0.5 mg L⁻¹, initial caffeine concentration = 5–10 mg L⁻¹	232.56	1.36	Langmuir	Pseudo-second-order	—	Surface complexation, hydrogen bonding, electrostatic interaction, and van der Waals force	185
Agricultural waste-based materials (activated carbon derived from olive stones)	Pyrolysis method	Surface: BET Structural morphology: SEM, EDS Others: pHPZC	Amoxicillin	1174.00	At 25 °C, pH 7, contact time = 4000 min, initial adsorbent dosage = 1 g L⁻¹, initial caffeine concentration = 12.5–100 mg L⁻¹	67.7	0.058	Sips	Pseudo-second-order	—	Chemisorption	186
Naturally occurring materials (chitosan-grafted	Co-precipitation method	Surface: BET Adsorption quantification: UV-vis	Ciprofloxacin	126.16	At 37 °C, pH 7,4, contact time = 2 h, initial adsorbent dosage = 1–10 mg L⁻¹, initial ciprofloxacin	100.74	0.79	Langmuir	Pseudo-second-order	—	Monolayer mechanism	136

Table 4 (*Contd.*)

Adsorbent	Synthesis techniques	Characterization techniques	Adsorbate	Surface area ($m^2\ g^{-1}$)	Experimental conditions	Maximum experimental adsorption capacity ($mg\ g^{-1}$)	Adsorption capacity per unit surface area ($mg\ m^{-2}$)	Adsorption isotherm	Adsorption kinetics	Thermodynamic parameters (ΔG kJ mol^{-1}, ΔH kJ mol^{-1}, and ΔS J mol^{-1} K^{-1})	Key insights	Reference
SiO$_2$–Fe$_3$O$_4$)		Structural morphology: SEM Others: FTIR, XRD, zeta potential, TGA, vibrating sample magnetometer			concentration = 12.5–10 mgL^{-1}							
Naturally occurring materials (NiFe$_2$O$_4$–COF-chitosan-terephthalaldehyde nanocomposites film)	Hydrothermal method	Surface: BET Structural morphology: SEM, TEM, HR-TEM, EDX Others: FTIR, XRD, TGA, elemental analysis	Tetracycline	107.33	At 25 °C, pH 3–11, contact time = 30 min, initial adsorbent dosage = 5.4 mg, initial tetracycline concentration = 10 to 400 mg L^{-1}	388.52	3.62	Freundlich	Pseudo-second-order	—	Complexation, cation exchange, electrostatic attraction, hydrogen bonding, and the π–π interaction	137
Naturally occurring materials (magnetically engineered sulfurized peat-based activated carbon)	Pyrolysis method	Surface: BET Structural morphology: SEM, EDS Others: FTIR, XPS, XRD, zeta potential	Sulfamethoxazole (SMX)	724	At 311 K, pH 11, contact time = 30 min, initial adsorbent dosage = 5.4 mg L^{-1}, initial sulfamethoxazole (SMX) concentration = 1.4 mg L^{-1}	94%		Langmuir (linear) and Freundlich (non-linear) isotherms	Pseudo-second-order	—	π–π electron donor–acceptor interactions, hydrogen bonding	138
Naturally occurring materials (bark-based biochar)	Pyrolysis method	Surface: BET Structural morphology: SEM Others: FTIR, pHPZC	Tetracycline	683.33	At 10–50 °C, pH 2–12, contact time = 10–120 min, initial adsorbent dosage = 1–2 g L^{-1}, initial tetracycline concentration = 50–500 mg L^{-1}	58.47	0.085	Langmuir	Pseudo-second-order	—	Chemisorption	187

be classified into conventional commercial adsorbents and non-conventional waste-generated adsorbents. Despite being favored by traditional adsorbents for contaminant removal, the extensive industrial application of these commercial materials is constrained by their high cost. Natural materials (Fuller's earth or bauxite, wood, sawdust), natural materials treated to develop their structures and properties (activated alumina, activated carbon, silica gel), manufactured materials (zeolites, polymeric resins, aluminosilicates, *etc.*), agricultural solid wastes and industrial byproducts (red mud, fly ash or date pits), and biosorbents (bacterial biomass, fungi or chitosan) are the five classes of adsorbents.[118] In recent decades, adsorbents for water treatment that are affordable, environmentally responsible, and easy to design have become increasingly popular. Table 4 presents the adsorption capacities, specific surface areas, adsorption conditions, adsorption kinetics, and isotherms, as well as potential mechanisms for the removal of pharmaceutical wastewater using some sustainable adsorbents.

5.5.1 Biochar as an adsorbent. Biochar is a unique substance for treating wastewater due to its ecologically benign and adaptable properties. Biochar has proven to be a successful approach for absorbing colorants that may be hazardous and detrimental to the environment due to its adsorption abilities. Biochar and composites made of it have recently come to light as adsorbents that are both very efficient and cost-effective, especially when it comes to treating pharmaceutical wastewater because of their notable characteristics, including a large surface area, a variety of capabilities, sustainability, and adjustable attributes. Fig. 8 illustrates the entire process of biomass production and modification methods from various sources, as well as the mechanism of adsorption of pharmaceutical pollutants.

The highest concentrations of pharmaceutical pollutants recovered with biochar include tetracycline (found at 1163 mg g^{-1}), sulfamethoxazole (found at 400 mg g^{-1}), naproxen (596 mg g^{-1}), and norfloxacin (698.6 mg g^{-1}) when using biochar derived from corncobs.[118] Unlike other adsorbents, biochar can be recycled up to eight times with minimal efficiency loss.[118] Additionally, hazelnut shell was utilized as a precursor in producing magnetic biochar (MBC), which was subsequently applied as a biosorbent to eliminate pharmaceutical impurities from contaminated water. This hazelnut shell biochar achieved the highest Pen-G adsorption capacity of 479 mg g^{-1} at 40 °C, pH 2, 1000 ppm penicillin-G (Pen-G) concentration, and 0.175 g of adsorbent per 100 g of solution.[120] Iron-loaded sludge biochar showed excellent performance, with a surface area of 82.78 m^2 g^{-1}, removing tetracycline (TC) to a maximum adsorption capacity of 104.86 mg g^{-1} under pH levels of 2–10.[121] Furthermore, biosolid (mostly biowaste)-derived biochar has an excellent surface area of approximately 182 m^2 g^{-1} and removed triclosan from wastewater with a capacity of about 1330 µg g^{-1} at pH 7.[122] Sewage sludge-derived biochar also showed excellent potential for wastewater treatment as it removed diclofenac (DCF), naproxen (NAP), and triclosan (TCS) with maximum adsorption capacities of 92.7 mg g^{-1}, 127 mg g^{-1}, and 113 mg g^{-1}, respectively, from polluted water at pH 2–11.[123] Biochar generated from maple leaves at three temperatures (350 °C, 550 °C, and 750 °C) produced the highest sorption rate for tetracycline, with an adsorption capacity of 407.3 mg g^{-1} at a pyrolytic temperature of 750 °C.[124] Algal-based (*Spirulina* species) biochar generated at a temperature of 750 °C was shown to be more effective in treating tetracycline waste than biochar generated at 350 °C and 550 °C, with an adsorption potential of 132.8 mg g^{-1}.[125] Sulfadiazine, sulfamethazine, and sulfachloropyridazine can all be removed by walnut shell biochar with removal efficiencies of 32 mg g^{-1}, 46 mg g^{-1}, and 40 mg g^{-1}, respectively.[126] Sulfamethoxazole was significantly removed from biochar made from sugarcane bagasse by hydrothermal carbonization at 200 °C and alkali activation with NaOH in an inert environment. A maximal sorption capacity of 400 mg g^{-1} was reported by Prasannamedha *et al.*[127] Novel biochar derived from corn stalk, reed stalk, and willow branches
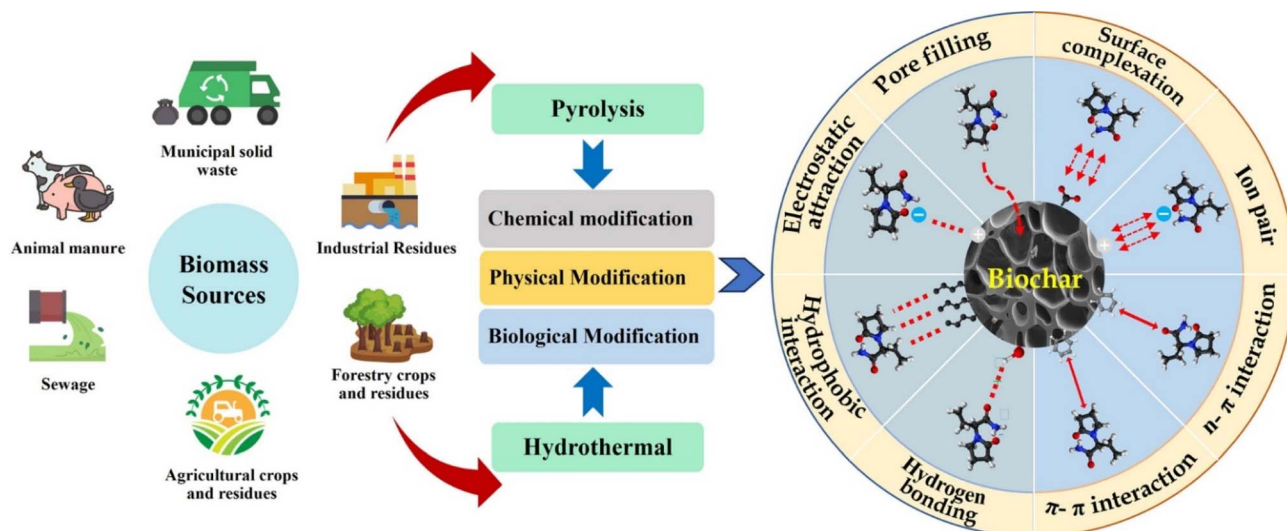

Fig. 8 Biochar production and modification using various sources for the adsorption and elimination of pharmaceutical contaminants from wastewater (adapted from ref. 119 with permission from Elsevier, copyright 2024).

was studied by Wang *et al.*,[128] and used for norfloxacin removal in water, achieving maximum adsorption capacities of 7.2469, 3.5139, and 6.2587 mg g^{-1}, respectively. Moreover, peanut shell-derived biochar, which was prepared by pyrolysis at 800 °C for approximately 4 hours, removed naproxen with an excellent adsorption capacity of 324 mg g^{-1}.[129]

5.5.2 Agricultural waste-based carbon materials as adsorbents. Waste management is a problem that must be addressed more. Due to its relatively high fixed carbon content and porous structure, this inexpensive and plentiful agricultural waste might be investigated as a low-cost alternative adsorbent.[130] Several researchers have recently concentrated their efforts on investigating alternative agricultural waste-based carbon sources to synthesize activated carbon.[131] Naproxen, diclofenac, ibuprofen, and ketoprofen were adsorbed using activated carbon from olive waste.[132] Portinho *et al.* investigated the use of adsorbent made from grape stalk, a byproduct from industrialization process, for caffeine removal by adsorption.[133] An additional agricultural waste, banana pseudo-stem, is used to remove amoxicillin.[134] Additionally, norfloxacin pharmaceutical pollutant was removed by shaddock peel, which is produced *via* hydrothermal carbonization (HTC) pre-treatment, with a maximum adsorption capacity of 746.29 mg g^{-1}.[135] The authors demonstrated that the adsorbent's increased porosity and surface area were related to its excellent adsorption performance.

5.5.3 Naturally occurring materials as adsorbents. Many natural materials have the potential to be used as adsorbents. They are available in large quantities in our environment, often at low cost, and can remove various pollutants from wastewater. Natural adsorbent chitosan-grafted SiO_2–Fe_3O_4 removed ciprofloxacin from wastewater with a sorption capacity of 100.74 mg g^{-1}.[136] Again, another adsorbent, $NiFe_2O_4$–COF–chitosan terephthalaldehyde nanocomposites (NCCT), has great potential for removing pharmaceutical pollutant tetracycline from wastewater. Li *et al.* demonstrated that the adsorption mechanism for these pollutants was likely due to electrostatic and π–π interactions, ion exchange, complexation, and hydrogen bonding.[137] Peat is another naturally occurring material containing lignin and cellulose as significant constituents that can be used as a sustainable source of biomass for producing activated carbon/biochar. According to Shukla *et al.*,[138] caffeine and sulfamethoxazole (SMX) were adsorbable on magnetically engineered sulfurized peat-based activated carbon (MEPBAC) from aqueous medium. Another study introduced magnetite-pine bark and iron-modified peat as effective, affordable, and environmentally friendly biosorbents for removing pharmaceutical contaminants like levofloxacin and trimethoprim from wastewater.[139] Another study described an optimization process for obtaining the best adsorbent from four tannin feedstocks: *Acacia mearnsii de Wild*, *Schinopsis balansae*, *Cupressus sempervirens*, and *Pinus pinaster* bark extract, all of which are highly effective at removing specific contaminants, such as the pharmaceutical species trimethoprim.[140] Peat has been studied as an adsorbent by various researchers.[141]

5.5.4 Industrial waste-based materials as adsorbents. A massive amount of solid and semisolid waste is produced by many industries daily all over the world. This industrial waste can be utilized as an adsorbent for wastewater treatment, which

can be obtained at almost no cost. Numerous industrial wastes have been researched as adsorbents for removing contaminants from wastewater, either with or without treatment. Fly ash—a byproduct from coal combustion—is an excellent alternative to activated carbon or zeolites for wastewater treatment with significant promise in environmental applications. Fly ash has significant physicochemical properties like particle size, density, porosity, surface area, and water holding capacity, with the chemical properties of silica (60–65%), alumina (25–30%), magnetite, and Fe_2O_3 (6–15%), which make it an appropriate choice for use as an adsorbent. Cost and efficiency are significant obstacles to introducing a sorbent into the commercial sector. Efforts have been made to create adsorption-capable zeolites from coal fly ash (CFA), the waste product of coal power plants. To achieve the highest removal effectiveness, the influences of pH, concentration, and external salt were also investigated.[142] A nanosized Fe_0/FeS_x composite (Fe_0/FeS_x@BFS) supported by blast furnace slag was created and employed for the *in situ* treatment of groundwater contaminated with oxytetracycline (OTC).[143] Senar Aydın *et al.* looked at the simple and efficient removal of psychiatric medications from wastewater treatment plant effluents using magnetite red mud nanoparticles.[144] In their work, manufactured magnetite red mud nanoparticles (RM-NPs) were used for the first time to remove psychiatric medications (fluoxetine, paroxetine, carbamazepine, diazepam, and lorazepam) from WWTP effluent. The removal efficiencies of anti-inflammatory drugs (AAIDs) from magnetite nanoparticles made from red mud (mNPs-RM) ranged from 90% (diclofenac) to 100% (naproxen, codeine, and indomethacin).[145]

5.5.5 Biosorbents. A relatively new development is using biological materials to remove contaminants from effluents. Researchers' interest in biomaterials made from proteins has grown in recent years due to their extensive use in various goods. To increase their ability to remove pharmaceutically active compounds (PACs) from the water system, several biosorbents have been altered. Due to their natural origin, biodegradability, simplicity of modification, and reliance on renewable resources, biosorbents have attracted attention for application in water treatment. Waste products have also been used as feedstocks to create biosorbents.[146] *Scenedesmus obliquus* (alga) was studied by Ali *et al.* as a potential adsorbent for the removal of pharmaceutical compounds (cefadroxil, paracetamol, ibuprofen, tramadol, and ciprofloxacin) from water.[147] Another biosorbent, sisal waste, was chemically activated to create activated carbon, which has tremendous potential for removing ibuprofen and paracetamol.[148] Khazri *et al.* investigated the adsorption of two commonly found drugs in surface waters, atenolol, and clarithromycin, onto cuttlefish bone powder that was successfully treated with HCl.[149]

6 Sustainable management of used adsorbents

The adsorbent materials reviewed in this work can be broadly categorized into five main types: metal–organic frameworks

(MOFs), graphene/graphene-based materials, zeolites, metal oxide nanoparticles, and biochar. Table 5 presents the sustainability of using these materials, based on their carbon footprint, E-factor, and life cycle assessment (LCA) outcomes for material synthesis. It is worth noting that there is significant variability in the reviewed metrics within each class of materials, due to variations in chemical compositions and synthesis techniques. For instance, Dutta et al. reported that MOF-88 (Zr) has a carbon footprint of 2482 kg CO_2 eq., whereas CAU-10 has only 23.7 kg CO_2 eq. global warming potential.[188] Meanwhile, the carbon footprint of zeolite is dependent on the gel composition and crystallization of the material.[189] As presented in Table 5, the mass ratio between the waste and desired product, i.e., the E-factor, is low for graphene oxide materials, but the carbon footprint is relatively high, resulting in a high LCA outcome. Although conventional synthesis of MOF generally produces a significant amount of waste, green sources such as waste-derived materials can drastically reduce the E-factor. The overall sustainability of the reviewed adsorbent materials follows the order MOFs < graphene-based materials < zeolites < metal oxide nanoparticles < biochar. As such, our review takes a top-down approach with the least sustainable material (i.e., MOFs) discussed first and biochar last.

After removing pollutants, adsorbents with high aquatic stability may readily separate from wastewater streams. The reusability of used adsorbents is determined by their capacity for recovery, decontamination, and regeneration. The adsorbent needs to be reused and regenerated to reduce costs for industrial applications. The regeneration method must be chosen carefully to effectively desorb the pollutant. The viability of industrial-scale use depends on several factors, including the kind of adsorbent, the contaminants, the adsorbent's stability, the toxicity of the used adsorbents, and the cost and energy requirements of the regeneration process. Filtration, magnetic separation, thermal desorption, microwave irradiation, advanced oxidation process, solvent regeneration, and microbial-assisted adsorbent regeneration are several techniques for regenerating spent adsorbent. A bar magnet can readily separate magnetic biochar from biomass that has been pre-treated with iron salts like $K_2Fe_2O_4$ and $FeCl_2/FeCl_3$ to create magnetic biochar.[190] An adsorbent created by coating palygorskite with magnetite nanoparticles displayed a magnetic susceptibility of 20.2 emu g^{-1} and absorbed 26.6 mg g^{-1} of Pb^{2+} from water. The spent adsorbent was easily separated using a basic bar magnet.[191] An et al. showed the potential for excellent sorbent reusability.[192] Up to the fifth run, the number of MOF-derived carbons (MDCs) required to remove pharmaceutical products from water did not significantly grow as the number of cycles increased. Moreover, the performance was still around an order of magnitude higher than the brand-new activated carbon (AC) after the fifth run. Furthermore, metal recovery by thermal desorption from used adsorbent is an emerging method. MWCNT (multi-walled carbon nanotubes) were successfully recycled by Toński et al. by thermal desorption, and effectively used to remove cyclophosphamide, ifosfamide, and 5-fluorouracil.[193] Using 0.5 M NaOH, arsenic could be desorbed from magnetic sorbents, and additional magnetic

Table 5 Sustainability of the different categories of adsorbent materials studied in this work

Adsorbent category	Cost of material	Regeneration potential	Carbon footprint (kg CO_2 eq. kg^{-1} adsorbent)	E-factor (kg of waste/kg of desired product)	Lifecycle assessment outcome	Techno-economic analysis based on capital expenditure (CAPEX) and operating expenditure (OPEX)
Metal–organic frameworks	$20–50 kg^{-1} (ref. 197 and 198)	Typically limited (<5 cycles); stability issues[199]	23.7–2482 (ref. 188)	1.3–19.9 (ref. 200)	Very high, as the carbon footprint is substantial	Scaling is limited due to very high CAPEX and OPEX[197,198]
Graphene/graphene oxides	$10–25 kg^{-1} (ref. 201)	Moderate; potential loss due to oxidation[202]	60–594 (ref. 188)	0.1–2.5 (ref. 203)	High due to its high global warming potential/carbon footprint	Moderately scalable as OPEX is moderate[201]
Zeolites	$2–4 kg^{-1} (ref. 204)	Good, thermally stable[205]	1–15 (ref. 189)	21 (ref. 206)	Moderate due to its moderate carbon footprint	Highly scalable as it requires low CAPEX and OPEX[204]
Metal oxide nanoparticles	$5–50 kg^{-1} (ref. 116)	Typically, 5–10 cycles with >85–95% capacity retention[207]	9.9×10^{-2}–3.7 (ref. 208)	2.1–15 (ref. 209)	Lower due to its low carbon footprint value	OPEX is moderate, and scaling is moderate[116]
Biochar	Less than $1 kg^{-1} (ref. 210)	5–8 cycles depending on surface functionalization[211]	−6.3–1 (ref. 212)	1.4 (ref. 213)	Negative as these are mainly produced from carbon sources and possess low end-of-life risk	Highly scalable due to having the lowest CAPEX and OPEX values compared to the other adsorbent categories[210]

adsorbents could be regenerated, as demonstrated by Baig et al.[194] When used as regeneration solvents, HCl, HNO$_3$, and H$_2$SO$_4$ showed considerable desorption efficiency.[195] Advanced oxidation processes (AOPs) for regenerating used adsorbents have gained popularity in recent years. Yang et al. studied the bio-regeneration of clays or functionalized clays and reported that microbial regeneration of montmorillonite functionalized with hexadecyltrimethylammonium (HDTMA) was superior to chemical regeneration.[196]

Environmental and societal problems might result from the open disposal of used adsorbents that contain harmful organic pollutants, especially in developing countries with limited access to designed landfills and incinerators. That is why the management of spent sorbents is significant. Although disposal is a cost-effective method, it is crucial to consider its environmental viability and long-term sustainability. Four methods (reuse, regeneration, repurposing/recycling, and final disposal) have been utilized for the sorbent's management, disposal, and repurposing. While landfilling and incineration are standard safe disposal methods, reused waste adsorbents are employed in applications including soil amendment, capacitors, and catalyst/catalyst support.

7 Process intensification in adsorptive wastewater treatment

Process intensification (PI) strategies are crucial for enhancing efficiency, reducing costs, and minimizing the environmental footprint of adsorption processes in pharmaceutical wastewater treatment. These approaches involve innovative reactor designs, integration with other treatment methods, and advanced operational techniques to overcome the limitations of conventional batch systems. This section discusses key PI strategies, including fluidized-bed adsorbers, hybrid adsorption–biological systems, modular reactor designs, and their challenges and prospects for industrial implementation.

7.1 Fluidized-bed adsorbers

Fluidized-bed reactors (FBRs) significantly outperform fixed-bed systems by enhancing mass transfer and enabling continuous operation. In FBRs, adsorbent particles (e.g., granular activated carbon, zeolite composites, or biochar) are suspended in an upward-flowing wastewater stream, which maximizes contact efficiency and minimizes clogging.[214] The fluidized state also facilitates in situ regeneration by allowing periodic introduction of regenerants without halting the process. However, challenges include controlling fluidization velocity to prevent particle attrition and ensuring uniform adsorbent distribution, which requires careful design and computational fluid dynamics modeling.

7.2 Hybrid adsorption–biological systems

Integrating adsorption with biological treatment creates synergistic effects that enhance removal efficiency and sustainability. Adsorbents, such as powdered activated carbon (PAC) or biochar, protect microbial communities from toxic pharmaceuticals by sequestering inhibitory compounds, while biological activity degrades the adsorbed pollutants, thereby extending the life of the adsorbent. A pilot-scale study by Kim et al. showed that a hybrid system combining activated biochar with an ultrafiltration membrane (ABC-UF) increased the removal of ibuprofen, carbamazepine, and 17α-ethinyl estradiol by 17–38% compared to UF alone, without significant flux reduction.[215] Similarly, microbial-assisted regeneration of adsorbents, such as hexadecyltrimethylammonium (HDTMA)-functionalized clays, has proven more effective than chemical regeneration.[216] Key challenges include managing biofilm formation on adsorbent surfaces and adapting to variable wastewater compositions, necessitating real-time monitoring and adaptive control strategies.

7.3 Modular and advanced reactor designs

Modular reactor designs offer flexibility and scalability for decentralized or point-of-use pharmaceutical wastewater treatment. Rotating adsorbent contactors (RACs) and electro-adsorption modules exemplify such innovations. RACs employ discs coated with adsorbent materials (e.g., graphene-MOF composites) that rotate through wastewater, providing high surface area contact and easy regeneration.[217] Electro-adsorption utilizes electric fields to enhance the uptake of ionizable pharmaceuticals on conductive adsorbents (e.g., graphene-based electrodes), followed by electrochemical regeneration. Despite their promise, these systems face challenges related to scaling up, including material durability under hydraulic stress and optimizing energy consumption.

7.4 Scale-up challenges and sustainability assessment

Scaling adsorption processes requires addressing hydrodynamic complexities, adsorbent stability, and cost-effectiveness. Multiscale modeling (e.g., computational fluid dynamics coupled with adsorption kinetics) is crucial for optimizing reactor geometry and flow patterns to minimize dead zones and maximize contact efficiency.[218] Adsorbent durability can be improved through pelletization (e.g., MOF-alginate beads) or embedding in polymer matrices, which prevent fragmentation. Economically, waste-derived adsorbents (e.g., fly ash–zeolite composites) reduce material costs significantly when regenerated in situ. Sustainability must be quantified via life cycle assessment (LCA) and techno–economic analysis (TEA). Therefore, future efforts should standardize these metrics to facilitate benchmarking of PI technologies.

8 Future outlook

Over the last two decades, numerous research and review articles have been published on ecotoxicology and the removal of pharmaceutical pollutants. These works have been pivotal in our understanding of PW. However, a few research gaps still need to be addressed.

A synergistic effect on reproduction in natural surface water containing a quaternary mixture of FLU, metformin, ASA, and CIP was reported by Tominaga et al.[219] In a mixture, the

pollutants can exhibit independent mechanisms (independent action model) or a common mechanism (all pollutants show the same effect with a precise mechanism, concentration action model). Hence, more studies should focus on the ecotoxicological effects of pharmaceutical pollutants in mixtures. It emphasizes the importance of conducting ecotoxicological studies under more realistic conditions and considering the interactions between PWs. Furthermore, in most studies, the treatment process and performance have been highlighted, while the toxicity assessment of the treated wastewater has been overlooked. The treated water may still be ecologically toxic. Furthermore, the possibility of secondary pollution by the adsorbent (e.g., metal ion leaching from perovskites) and transformed products generated during the treatment process should not be overlooked. Research related to PW treatment should include toxicity tests to validate the performance of the proposed treatment method.

Over the last two and a half decades, numerous articles have been published on the removal of pharmaceutical pollutants through adsorption. However, less than 5% of these works have investigated competitive adsorption.[220] In the practical environment, various pharmaceutical pollutants are expected to be present in wastewater at varying concentrations. Investigators should consider this reality in future projects. This mixture of different pollutants also presents a challenge in designing adsorbents. Since different active ingredients contain distinct functional groups in their structures, the adsorption efficacy regarding a single target compound may vary depending on the adsorbent. The synthesis of green materials containing various functional groups that can adsorb multiple pollutants can be an interesting topic to explore in the future. At the same time, researchers should focus on performing regeneration studies of these materials for waste minimization and cost optimization.

Since pharmaceutical pollutants (PPs) are emerging contaminants, existing wastewater treatment plants may have lower pollutant removal efficiencies. However, utilizing the existing treatment infrastructure and modifying these already established facilities will be more economical and time-consuming. Integrating multiple processes with the existing ones can improve performance.[221,222] Adsorption of IBU, CAR, and 17 α-ethinyl estradiol (EE2) using activated biochar (ABC) followed by an ultrafiltration (UF) membrane increased the retention rate to 41.8%, 40.9%, and 53.0% from 24.4%, 7.0%, and 14.8%, respectively, in a UF alone system without decreasing the flux rate considerably (normalized flux rate in ABC = 0.85).[215] Approximately 10% more COD removal from a pharmaceutical industrial effluent containing anti-psychotic and anti-cancer ingredients was achieved using advanced oxidation (ozone + peroxide)-activated char treatment (85.4%) than oxidation alone (75%) at pH 5.[223] A combined activated sludge–activated carbon system removed 100% (2 mg L^{-1} each) of acetaminophen, IBU, and caffeine, showing better results than the biological treatment alone. More studies should focus on hybrid treatment methods for efficiently removing pharmaceutical components from wastewater.[224]

Although adsorption has been reported as an efficient method for PP removal from wastewater, laboratory results do not represent the practical pilot-scale/actual performance of the treatment process. Since wastewater has a highly complex character, accurately simulating wastewater in the lab is rarely attainable. It hinders the evaluation of the actual performance of the adsorbent. Additionally, further adsorption studies of various materials, such as perovskites, should be conducted in practical settings. The performance and cost of treatments performed in a laboratory setting can differ significantly in real-life applications. Further pilot-scale studies are needed to develop more robust, efficient, and cost-effective treatment methods.

Techno-economic analysis (TEA) is a crucial tool for evaluating the feasibility of industrial processes. TEA of the adsorptive treatment of pharmaceutical wastewater is scarce. Echevarría et al.[225] performed TEA on an advanced water reclamation pilot plant operating at a capacity of 1.5–2 m^3 h^{-1}. Two ultrafiltration-reverse osmosis (UF-RO) blends, including only RO and a powdered activated carbon (PAC)-tight UF, were evaluated for treating wastewater containing CAR, DIC, ERY, SUL, and diuron. PAC-tight UF showed 81 $\pm$ 13% removal efficiency, while 55 $\pm$ 11% pollutants were removed by UF-RO (50% blend). UF-RO (50%) required the lowest operating cost at €0.18 m^{-3}, followed by PAC-tight UF (€0.22 m^{-3}; 20 mg L^{-1} PAC), 25% UF-RO (€0.24 m^{-3}), and OR (€0.31 m^{-3}). The lowest capital expenditure of €548 m^{-3} was estimated for PAC-tight UF, while 50% UF-RO, 25% UF-RO, and RO would cost €594 m^{-3}, €628 m^{-3}, and €662 m^{-3}, respectively. As the ecological threat of PPs is mounting, the necessity of more techno–economic studies in this regard has become paramount. The techno–economic feasibility of resource recovery (e.g., pharmaceutical precursors) from PW can be a predominant research direction to ensure the robustness of future treatment plants.

9 Conclusions

Pharmaceuticals are complex chemical compounds that can persist in the environment and are not easily eliminated by traditional wastewater and drinking water treatment methods. Although present at low concentrations, their impact on aquatic life and human health raises concerns about the long-term effects. Several ongoing investigations are underway to detect these compounds in wastewater and develop viable technologies for their removal. Adsorption is a less-expensive alternative that has been studied for the removal of several pharmaceuticals and has demonstrated excellent efficiency in removing a wide range of organic and inorganic pharmaceutical substances. Some of the interacting mechanisms that can lead to the adsorption of a specific pharmaceutical include electrostatic interactions, protonation, ion exchange, dipole–dipole interactions, H-bonding, and complex formation. Various operating parameters, including ionic strength, pH, adsorbent dosage, initial concentration of the pharmaceutical, temperature, and the presence of secondary solute components, greatly influence the adsorption of pharmaceuticals from wastewater. Nevertheless, adsorption requires substantial quantities of adsorbent, which must be either recycled or discarded after use. It is also imperative that the retrieved drugs and their

derivatives are disposed of properly. Cost-effective and efficient adsorbents for treating pharmaceutical wastewater on a large scale are still highly desired, after considering all the influencing factors and numerous advantages and disadvantages of different adsorbents. Therefore, there is a pressing need to develop next-generation adsorbents that are sustainable, innovative, benign, and capable of removing emerging contaminants at trace levels with enhanced affinity, capacity, and selectivity. Therefore, future efforts should be directed towards investigating the ecotoxicological impact, removal efficacy, and competitive adsorption in multi-adsorbate pharmaceutical wastewater, scaling up laboratory research work to the pilot-scale and subsequently industrial applications, the hybridization of multiple wastewater treatment techniques, and conducting techno–economic analysis to ensure the feasibility of the discussed adsorbent materials for practical applications.

Author contributions

Sadia Sharmin Sporsho: writing – original draft, formal analysis, conceptualization, review & editing. Dipu Saha: writing – original draft, formal analysis, data curation, review & editing. Mahmudul Hasan Khan: writing – original draft, formal analysis. Md Shahriar Rahman: writing – review & editing. Mahe Rukh: writing – original draft. Faysal Haque: writing– original draft. Md Reazul Islam: writing – original draft. Tulie Chakma: writing – original draft. Hridoy Roy: writing – review & editing. Dipayan Sarkar: writing – original draft, data curation. Md. Shahinoor Islam: writing, review & editing, and Supervision.

Conflicts of interest

The authors declare no conflicts of interest.

Data availability

No new data was created or analyzed during this study. Data sharing does not apply to this article.

Acknowledgements

References

1 F. Malerba and L. Orsenigo, *Bus. Hist.*, 2015, **57**, 664–687.
2 C. G. Daughton, *Environ. Impact Assess. Rev.*, 2004, **24**, 711–732.
3 C. Gadipelly, A. Pérez-González, G. D. Yadav, I. Ortiz, R. Ibáñez, V. K. Rathod and K. V Marathe, *Ind. Eng. Chem. Res.*, 2014, **53**, 11571–11592.
4 R. Gupta, B. Sati and A. Gupta, *Advances in Biological Treatment of Industrial Waste Water and Their Recycling for a Sustainable Future*, 2019, pp. 267–302.
5 H. Imran, *Electron. J. Environ. Agric. Food Chem.*, 2005, **4**, 994–1004.
6 M. Martz, *Pharm. Eng.*, 2012, **32**, 1–12.
7 C. Zwiener, *Anal. Bioanal. Chem.*, 2007, **387**, 1159–1162.
8 Y. Li, S. Zhang, W. Zhang, W. Xiong, Q. Ye, X. Hou, C. Wang and P. Wang, *J. Environ. Manage.*, 2019, **238**, 442–450.
9 G. Wernet, S. Conradt, H. P. Isenring, C. Jiménez-González and K. Hungerbühler, *Int. J. Life Cycle Assess.*, 2010, **15**, 294–303.
10 K. Yang, B. Lv, H. Shen, G. Jing and Z. Zhou, *Int. J. Life Cycle Assess.*, 2021, **26**, 64–75.
11 B. Du, A. E. Price, W. C. Scott, L. A. Kristofco, A. J. Ramirez, C. K. Chambliss, J. C. Yelderman and B. W. Brooks, *Sci. Total Environ.*, 2014, **466**, 976–984.
12 Y. Yang, Y. S. Ok, K.-H. Kim, E. E. Kwon and Y. F. Tsang, *Sci. Total Environ.*, 2017, **596**, 303–320.
13 R. Parra-Saldivar, C. Castillo-Zacarías, M. Bilal, H. M. N. Iqbal and D. Barceló, *Interaction and Fate of Pharmaceuticals in Soil-Crop Systems: the Impact of Reclaimed Wastewater*, 2021, pp. 33–47.
14 H. Chen, Z. Tu, S. Wu, G. Yu, C. Du, H. Wang, E. Yang, L. Zhou, B. Deng, D. Wang and H. Li, *Chemosphere*, 2021, **278**, 130436.
15 M. Ibáñez, V. Borova, C. Boix, R. Aalizadeh, R. Bade, N. S. Thomaidis and F. Hernández, *J. Hazard. Mater.*, 2017, **323**, 26–35.
16 K. Kuroda, C. Li, K. Dhangar and M. Kumar, *Sci. Total Environ.*, 2021, **776**, 145740.
17 R. Mirzaei, M. Yunesian, S. Nasseri, M. Gholami, E. Jalilzadeh, S. Shoeibi and A. Mesdaghinia, *Sci. Total Environ.*, 2018, **619–620**, 446–459.
18 M. J. Klemes, L. P. Skala, M. Ateia, B. Trang, D. E. Helbling and W. R. Dichtel, *Acc. Chem. Res.*, 2020, **53**, 2314–2324.
19 G. R. Quadra, H. Oliveira de Souza, R. dos S. Costa, M. A. dos and S. Fernandez, *Environ. Sci. Pollut. Res.*, 2017, **24**, 1200–1218.
20 J. Xiang, M. Wu, J. Lei, C. Fu, J. Gu and G. Xu, *Ecotoxicol. Environ. Saf.*, 2018, **150**, 289–296.
21 O. V Enick and M. M. Moore, *Environ. Impact Assess. Rev.*, 2007, **27**, 707–729.
22 S. Akter, M. B. K. Suhan and M. S. Islam, *Environ. Nanotechnol. Monit. Manag.*, 2022, **17**, 100643.
23 S. Midassi, A. Bedoui and N. Bensalah, *Chemosphere*, 2020, **260**, 127558.
24 A. Talaiekhozani, S. Joudaki, F. Banisharif, Z. Eskandari, J. Cho, G. Moghadam and S. Rezania, *Int. J. Environ. Res. Publ. Health*, 2020, **17**, 1758.
25 I. Arslan-Alaton and S. Dogruel, *J. Hazard. Mater.*, 2004, **112**, 105–113.
26 L. A. Pérez-Estrada, S. Malato, W. Gernjak, A. Agüera, E. M. Thurman, I. Ferrer and A. R. Fernández-Alba, *Environ. Sci. Technol.*, 2005, **39**, 8300–8306.
27 L. Yang, L. E. Yu and M. B. Ray, *Water Res.*, 2008, **42**, 3480–3488.
28 J. Radjenović, M. Petrović and D. Barceló, *TrAC, Trends Anal. Chem.*, 2007, **26**, 1132–1144.

29 N. Suriyanon, J. Permrungruang, J. Kaosaiphun, A. Wongrueng, C. Ngamcharussrivichai and P. Punyapalakul, *Chemosphere*, 2015, **136**, 222–231.

30 L. Mahouachi, T. Rastogi, W.-U. Palm, I. Ghorbel-Abid, D. Ben Hassen Chehimi and K. Kümmerer, *Chemosphere*, 2020, **258**, 127213.

31 T. Rasheed, A. A. Hassan, M. Bilal, T. Hussain and K. Rizwan, *Chemosphere*, 2020, **259**, 127369.

32 M. Rukh, M. S. Rahman, K. M. N. Sakib, S. C. Pantha, S. Hasan, M. Jabeen and M. S. Islam, *Carbon Capture Science & Technology*, 2024, 12, p. 100217.

33 M. de Oliveira, B. E. F. Frihling, J. Velasques, F. J. C. M. Filho, P. S. Cavalheri and L. Migliolo, *Sci. Total Environ.*, 2020, **705**, 135568.

34 D. Z. Husein, R. Hassanien and M. F. Al-Hakkani, *Heliyon*, 2019, **5**, 8.

35 M. Grassi, G. Kaykioglu, V. Belgiorno and G. Lofrano, in *Emerging Compounds Removal from Wastewater: Natural and Solar Based Treatments*, G. Lofrano, Springer Netherlands, Dordrecht, 2012, pp. 15–37.

36 E. Mousset, W. H. Loh, W. S. Lim, L. Jarry, Z. Wang and O. Lefebvre, *Water Res.*, 2021, **200**, 117234.

37 Z.-A. Jennifer, A.-D. Sonia, E.-B. Francesca, F.-M. Nadia and M.-R. Suanny, *Water Sci. Technol.*, 2024, **90**, 2340–2351.

38 I. Ali, M. Asim and T. A. Khan, *J. Environ. Manage.*, 2012, **113**, 170–183.

39 J. R. De Andrade, M. F. Oliveira, M. G. C. Da Silva and M. G. A. Vieira, *Ind. Eng. Chem. Res.*, 2018, **57**, 3103–3127.

40 F. Mansouri, K. Chouchene, N. Roche and M. Ksibi, *Appl. Sci.*, 2021, **11**(14), 6659.

41 K. H. Hama Aziz, F. S. Mustafa, K. M. Omer and I. Shafiq, *Water Resour. Ind.*, 2023, **30**, 100227.

42 K. H. Hama Aziz, N. M. Fatah and K. T. Muhammad, *R. Soc. Open Sci.*, 2024, **11**(5), 232033.

43 K. H. Hama Aziz, F. S. Mustafa, M. A. H. Karim and S. Hama, *Mater. Adv.*, 2025, **6**, 3433–3454.

44 Preprint, https://www.desotec.com/en-us/purification-need/industries-we-help/pharmaceuticals.

45 Preprint, https://www.hyerainc.com/wastewater-treatment.

46 Preprint, https://norit.com/applications/water-treatment/wastewater.

47 X. Shi, K. Y. Leong and H. Y. Ng, *Bioresour. Technol.*, 2017, **245**, 1238–1244.

48 F. Zhao, F. Ju, K. Huang, Y. Mao, X.-X. Zhang, H. Ren and T. Zhang, *Sci. Total Environ.*, 2019, **651**, 2148–2157.

49 K. Słoczyńska, J. Orzeł, A. Murzyn, J. Popiół, A. Gunia-Krzyżak, P. Koczurkiewicz-Adamczyk and E. Pękala, *Aquat. Toxicol.*, 2023, **260**, 106554.

50 J. O. Eniola, R. Kumar, M. A. Barakat and J. Rashid, *J. Clean. Prod.*, 2022, **356**, 131826.

51 J. Guo, L. Fortunato, B. J. Deka, S. Jeong and A. K. An, *Desalination*, 2020, **475**, 114148.

52 A. Jelić, M. Gros, M. Petrović, A. Ginebreda and D. Barceló, *Emerging and Priority Pollutants in Rivers*, 2012, 1–23.

53 M. S. Kostich, A. L. Batt and J. M. Lazorchak, *Environ. Pollut.*, 2014, **184**, 354–359.

54 L. M. Bexfield, P. L. Toccalino, K. Belitz, W. T. Foreman and E. T. Furlong, *Environ. Sci. Technol.*, 2019, **53**, 2950–2960.

55 P. M. Bradley, C. A. Journey, D. T. Button, D. M. Carlisle, B. J. Huffman, S. L. Qi, K. M. Romanok and P. C. Van Metre, *PLoS One*, 2020, **15**, e0228214.

56 Y. Lester, H. Mamane, I. Zucker and D. Avisar, *Water Res.*, 2013, **47**, 4349–4356.

57 R. Thakura, S. Chakrabortty and P. Pal, *Clean Technol. Environ. Policy*, 2015, **17**, 2299–2310.

58 R. Changotra, H. Rajput and A. Dhir, *J. Photochem. Photobiol., A*, 2019, **376**, 175–184.

59 K. K. Ng, X. Shi, M. K. Y. Tang and H. Y. Ng, *Sep. Purif. Technol.*, 2014, **132**, 634–643.

60 K. K. Ng, X. Shi and H. Y. Ng, *Water Res.*, 2015, **81**, 311–324.

61 Y. Kaya, A. M. Bacaksiz, H. Bayrak, Z. B. Gönder, I. Vergili, H. Hasar and G. Yilmaz, *Chem. Eng. J.*, 2017, **322**, 293–301.

62 A. T. Akarsubasi, O. Ince, B. Kirdar, N. A. Oz, D. Orhon, T. P. Curtis, I. M. Head and B. K. Ince, *Water Res.*, 2005, **39**, 1576–1584.

63 H. Al Qarni, P. Collier, J. O'Keeffe and J. Akunna, *Environ. Sci. Pollut. Res.*, 2016, **23**, 13003–13014.

64 C. Kantar, O. Oral and N. A. Oz, *Chemosphere*, 2019, **237**, 124440.

65 L. Wiest, T. Chonova, A. Bergé, R. Baudot, F. Bessueille-Barbier, L. Ayouni-Derouiche and E. Vulliet, *Environ. Sci. Pollut. Res.*, 2018, **25**, 9207–9218.

66 Z. Xing, D. Sun, X. Yu, J. Zou and W. Zhou, *Environ. Prog. Sustain. Energy*, 2014, **33**, 170–177.

67 F. Prestinaci, P. Pezzotti and A. Pantosti, *Pathog. Glob. Health*, 2015, **109**, 309–318.

68 M. Mohammadzadeh, A. Bello, S. B. Lassen, K. K. Brandt, S. Risteelä and T. Leiviskä, *Environ. Res.*, 2025, **268**, 120774.

69 A. Yamindago, N. Lee, N. Lee, Y. Jo, S. Woo and S. Yum, *Ecotoxicol. Environ. Saf.*, 2021, **227**, 112931.

70 E. Minagh, R. Hernan, K. O'Rourke, F. M. Lyng and M. Davoren, *Ecotoxicol. Environ. Saf.*, 2009, **72**, 434–440.

71 Z.-H. Li, V. Zlabek, R. Grabic, J. Velisek, J. Machova and T. Randak, *Ecotoxicology*, 2010, **19**, 872–878.

72 J. F. Henriques, A. R. Almeida, T. Andrade, O. Koba, O. Golovko, A. M. V. M. Soares, M. Oliveira and I. Domingues, *Aquat. Toxicol.*, 2016, **170**, 355–364.

73 M. Mezzelani, S. Gorbi, D. Fattorini, G. d'Errico, G. Consolandi, M. Milan, L. Bargelloni and F. Regoli, *Chemosphere*, 2018, **198**, 238–248.

74 M. Grzesiuk, J. Pijanowska, M. Markowska and A. Bednarska, *Environ. Pollut.*, 2020, **261**, 114135.

75 H. Cuiping, Z. Na, H. Limei, T. Tang, Y. Yang and N. Xiangping, *Ecotoxicology*, 2023, **32**, 137–149.

76 S. Rodrigues, S. C. Antunes, B. Nunes and A. T. Correia, *Ecotoxicol. Environ. Saf.*, 2019, **181**, 1–10.

77 M. J. Ahmed and B. H. Hameed, *J. Environ. Manage.*, 2019, **252**, 109617.

78 S. Azizian and S. Eris, in *Interface Science and Technology*, Elsevier, 2021, vol. 33, pp. 445–509.

79 M. Musah, Y. Azeh, J. T. Mathew, M. T. Umar, Z. Abdulhamid and A. I. Muhammad, *CaJoST*, 2022, **4**, 20–26.

80 J. Ouyang, L. Zhou, Z. Liu, J. Y. Y. Heng and W. Chen, *Sep. Purif. Technol.*, 2020, **253**, 117536.

81 J. Wang and X. Guo, *J. Hazard. Mater.*, 2020, **390**, 122156.

82 Y. Wang, C. Wang, X. Huang, Q. Zhang, T. Wang and X. Guo, *Chemosphere*, 2024, **349**, 140736.

83 J. Wang and X. Guo, *Chemosphere*, 2020, **258**, 127279.

84 X. Guo and J. Wang, *J. Mol. Liq.*, 2019, **296**, 111850.

85 D. Suteu and T. Malutan, *Bioresources*, 2013, **8**, 1.

86 J. Wang and X. Guo, *Chemosphere*, 2022, **309**, 136732.

87 K. H. H. Aziz, F. S. Mustafa and S. Hama, *Coord. Chem. Rev.*, 2025, **542**, 216875.

88 K. H. H. Aziz, F. S. Mustafa, R. F. Hamarawf and K. M. Omer, *J. Water Proc. Eng.*, 2025, **70**, 106867.

89 R. Zhang and P. Somasundaran, *Adv. Colloid Interface Sci.*, 2006, **123–126**, 213–229.

90 S. Kumar, S. Yadav, N. Kataria, A. K. Chauhan, S. Joshi, R. Gupta, P. Kumar, J. W. R. Chong, K. S. Khoo and P. L. Show, *Curr. Pollut. Rep.*, 2023, **9**, 110–142.

91 J. C. Jansen, J. H. Koegler, H. Van Bekkum, H. P. A. Calis, C. M. Van Den Bleek, F. Kapteijn, J. A. Moulijn, E. R. Geus and N. der Puil, *Microporous Mesoporous Mater.*, 1998, **21**, 213–226.

92 F. Izzo, M. Mercurio, B. de Gennaro, P. Aprea, P. Cappelletti, A. Daković, C. Germinario, C. Grifa, D. Smiljanic and A. Langella, *Colloids Surf., B*, 2019, **182**, 110380.

93 A. Martucci, L. Pasti, N. Marchetti, A. Cavazzini, F. Dondi and A. Alberti, *Microporous Mesoporous Mater.*, 2012, **148**, 174–183.

94 I. Braschi, S. Blasioli, L. Gigli, C. E. Gessa, A. Alberti and A. Martucci, *J. Hazard. Mater.*, 2010, **178**, 218–225.

95 J. Zhao, X. Yang, G. Liang, Z. Wang, S. Li, Z. Wang and X. Xie, *Sci. Total Environ.*, 2020, **710**, 136289.

96 P. Arabkhani, H. Javadian, A. Asfaram and M. Ateia, *Chemosphere*, 2021, **271**, 129610.

97 J. Liu, H. Lin, Y. Dong, Y. He, W. Liu and Y. Shi, *J. Environ. Chem. Eng.*, 2021, **9**, 105912.

98 T. M. Salem Attia, X. L. Hu and D. Q. Yin, *Chemosphere*, 2013, **93**, 2076–2085.

99 S. Zhong, S. Zhang, Y. Zhang and C. Li, *J. Mater. Sci.: Mater. Electron.*, 2019, **30**, 20410–20419.

100 Z. Hasan, J. Jeon and S. H. Jhung, *J. Hazard. Mater.*, 2012, **209–210**, 151–157.

101 S. Zhuang and J. Wang, *Chemosphere*, 2021, **281**, 130997.

102 M. R. Azhar, H. R. Abid, H. Sun, V. Periasamy, M. O. Tadé and S. Wang, *J. Colloid Interface Sci.*, 2016, **478**, 344–352.

103 M. R. Azhar, H. R. Abid, H. Sun, V. Periasamy, M. O. Tadé and S. Wang, *J. Colloid Interface Sci.*, 2016, **478**, 344–352.

104 H. Furukawa, K. E. Cordova, M. O'Keeffe and O. M. Yaghi, *Science*, 2013, **341**, 6149.

105 M.-S. Hosseini, A. Abbasi and M. Masteri-Farahani, *J. Hazard. Mater.*, 2022, **425**, 127975.

106 C. Yao, F. Che, X. Jiang, Z. Wu, J. Chen and K. Wang, *Chemosphere*, 2021, **267**, 128913.

107 A. Armano and S. Agnello, *C–J. Carbon Res.*, 2019, **5**, 67.

108 A. Anwar, B. S. Mohammed, M. A. Wahab and M. S. Liew, *Dev. Built Environ.*, 2020, **1**, 100002.

109 A. Anwar, B. S. Mohammed, M. A. Wahab and M. S. Liew, *Developments in the Built Environment*, 2020, **1**, 100002.

110 C. Kumunda, A. S. Adekunle, B. B. Mamba, N. W. Hlongwa and T. T. I. Nkambule, *Front. Mater.*, 2021, **7**, DOI: 10.3389/fmats.2020.616787.

111 T. T. Baby and S. Ramaprabhu, *J. Appl. Phys.*, 2010, **108**(12), 124308.

112 A. Saravanan, P. S. Kumar, S. Srinivasan, S. Jeevanantham, M. Vishnu, K. V. Amith, R. Sruthi, R. Saravanan and D.-V. N. Vo, *Chemosphere*, 2022, **298**, 134284.

113 S. Zhang, B. Li, X. Wang, G. Zhao, B. Hu, Z. Lu, T. Wen, J. Chen and X. Wang, *Chem. Eng. J.*, 2020, **390**, 124642.

114 P. Raizada, A. Sudhaik and P. Singh, *Mater. Sci. Energy Technol.*, 2019, **2**, 509–525.

115 I. M. Jauris, C. F. Matos, C. Saucier, E. C. Lima, A. J. G. Zarbin, S. B. Fagan, F. M. Machado and I. Zanella, *Phys. Chem. Chem. Phys.*, 2016, **18**, 1526–1536.

116 T. Naseem and T. Durrani, *J. Environ. Chem. Ecotoxicol.*, 2021, **3**, 59–75.

117 A. Ali, T. Shah, R. Ullah, M. Guo, M. Ovais, Z. Tan and Y. Rui, *Front. Chem.*, 2021, **9**, 629054.

118 G. Crini, E. Lichtfouse, L. D. Wilson and N. Morin-Crini, *Environ. Chem. Lett.*, 2019, **17**, 195–213.

119 K. H. Hama Aziz, F. S. Mustafa, M. A. Hassan, K. M. Omer and S. Hama, *Desalination*, 2024, **583**, 117725.

120 S. Aghagani and H. Baseri, *Urban Water J.*, 2022, **19**, 422–432.

121 J. Wei, Y. Liu, J. Li, Y. Zhu, H. Yu and Y. Peng, *Chemosphere*, 2019, **236**, 124254.

122 L. K. Kimbell, Y. Tong, B. K. Mayer and P. J. McNamara, *Environ. Eng. Sci.*, 2018, **35**, 513–524.

123 B. Czech, M. Kończak, M. Rakowska and P. Oleszczuk, *J. Clean. Prod.*, 2021, **288**, 125686.

124 J. E. Kim, S. K. Bhatia, H. J. Song, E. Yoo, H. J. Jeon, J.-Y. Yoon, Y. Yang, R. Gurav, Y.-H. Yang, H. J. Kim and Y.-K. Choi, *Bioresour. Technol.*, 2020, **306**, 123092.

125 Y.-K. Choi, T.-R. Choi, R. Gurav, S. K. Bhatia, Y.-L. Park, H. J. Kim, E. Kan and Y.-H. Yang, *Sci. Total Environ.*, 2020, **710**, 136282.

126 X. Geng, S. Lv, J. Yang, S. Cui and Z. Zhao, *J. Environ. Manage.*, 2021, **280**, 111749.

127 G. Prasannamedha, P. S. Kumar, R. Mehala, T. J. Sharumitha and D. Surendhar, *J. Hazard. Mater.*, 2021, **407**, 124825.

128 B. Wang, Y. Jiang, F. Li and D. Yang, *Bioresour. Technol.*, 2017, **233**, 159–165.

129 F. Tomul, Y. Arslan, B. Kabak, D. Trak, E. Kendüzler, E. C. Lima and H. N. Tran, *Sci. Total Environ.*, 2020, **726**, 137828.

130 A. Bhatnagar and A. Minocha, *Indian J. Chem. Technol.*

131 H. A. Alalwan, M. A. Kadhom and A. H. Alminshid, *J. Water Supply:Res. Technol.–AQUA*, 2020, **69**, 99–112.

132 D. T. Bankole, A. P. Oluyori and A. A. Inyinbor, *Arab. J. Chem.*, 2023, **16**, 104699.

133 R. Portinho, O. Zanella and L. A. Féris, *J. Environ. Manage.*, 2017, **202**, 178–187.

134 H. Chakhtouna, H. Benzeid, N. Zari, A. el kacem Qaiss and R. Bouhfid, *Sep. Purif. Technol.*, 2021, **266**, 118592.

135 X. Niu, C. Liu, L. Li, X. Han, C. Chang, P. Li and J. Chen, *Water Sci. Technol.*, 2022, **85**, 2964–2979.

136 S. T. Danalıoğlu, Ö. Kerkez Kuyumcu, M. Abdel Salam and Ş. S. Bayazit, *Environ. Sci. Pollut. Res.*, 2018, **25**, 36661–36670.

137 Z. Li, Y. Liu, S. Zou, C. Lu, H. Bai, H. Mu and J. Duan, *Chem. Eng. J.*, 2020, **382**, 123008.

138 V. Shukla, D. Panchal, O. Prakash, P. Mondal, I. Hiwrale, R. S. Dhodapkar and S. Pal, *Bioresour. Technol.*, 2023, **369**, 128399.

139 M. Mohammadzadeh and T. Leiviskä, *Ind. Crops Prod.*, 2023, **195**, 116491.

140 J. Beltrán-Heredia, P. Palo, J. Sánchez-Martín, J. R. Domínguez and T. González, *Ind. Eng. Chem. Res.*, 2012, **51**, 50–57.

141 P. A. Brown, S. A. Gill and S. J. Allen, *Water Res.*, 2000, **34**, 3907–3916.

142 S. H. Tumrani, R. A. Soomro, X. Zhang, D. A. Bhutto, N. Bux and X. Ji, *RSC Adv.*, 2021, **11**, 26110–26119.

143 R. Ding, P. Zhang, M. Seredych and T. J. Bandosz, *Water Res.*, 2012, **46**, 4081–4090.

144 S. Aydın, F. Bedük, A. Ulvi and M. E. Aydın, *Sci. Total Environ.*, 2021, **784**, 147174.

145 S. Aydın, A. Ulvi, F. Bedük and M. E. Aydın, *Water Air Soil Pollut.*, 2023, **234**, 384.

146 A. Adewuyi, *Water*, 2020, **12**, 1551.

147 M. E. M. Ali, A. M. Abd El-Aty, M. I. Badawy and R. K. Ali, *Ecotoxicol. Environ. Saf.*, 2018, **151**, 144–152.

148 A. S. Mestre, A. S. Bexiga, M. Proença, M. Andrade, M. L. Pinto, I. Matos, I. M. Fonseca and A. P. Carvalho, *Bioresour. Technol.*, 2011, **102**, 8253–8260.

149 H. Khazri, I. Ghorbel-Abid, R. Kalfat and M. Trabelsi-Ayadi, *Environ. Technol.*, 2018, **39**, 2662–2668.

150 H. H. Dang, D. T. C. Nguyen, T. T. Nguyen, T. T. T. Nguyen, D.-V. N. Vo, T. D. Nguyen, T. Lee and T. Van Tran, *J. Environ. Chem. Eng.*, 2021, **9**, 104938.

151 A. Martucci, M. A. Cremonini, S. Blasioli, L. Gigli, G. Gatti, L. Marchese and I. Braschi, *Microporous Mesoporous Mater.*, 2013, **170**, 274–286.

152 D. Capsoni, G. Guerra, C. Puscalau, F. Maraschi, G. Bruni, F. Monteforte, A. Profumo and M. Sturini, *Int. J. Environ. Res. Publ. Health*, 2021, **18**, 1433.

153 M. M. M. Ali, M. J. Ahmed and B. H. Hameed, *J. Clean. Prod.*, 2018, **172**, 602–608.

154 K.-Y. Andrew Lin, H. Yang and W.-D. Lee, *RSC Adv.*, 2015, **5**, 81330–81340.

155 D. Krajišnik, A. Daković, M. Milojević, A. Malenović, M. Kragović, D. B. Bogdanović, V. Dondur and J. Milić, *Colloids Surf., B*, 2011, **83**, 165–172.

156 A. Nezamzadeh-Ejhieh and A. Shirzadi, *Chemosphere*, 2014, **107**, 136–144.

157 D. Kanakaraju, J. Kockler, C. A. Motti, B. D. Glass and M. Oelgemöller, *Appl. Catal., B*, 2015, **166–167**, 45–55.

158 T. Van Tran, D. T. C. Nguyen, H. T. N. Le, D.-V. N. Vo, V.-D. Doan, V.-P. Dinh, H.-T. T. Nguyen, T. D. Nguyen and L. G. Bach, *C. R. Chim.*, 2019, **22**, 804–812.

159 T. Van Tran, D. T. C. Nguyen, H. T. N. Le, T. T. K. Tu, N. D. Le, K. T. Lim, L. G. Bach and T. D. Nguyen, *J. Environ. Chem. Eng.*, 2019, **7**, 102881.

160 Z. Hasan, E.-J. Choi and S. H. Jhung, *Chem. Eng. J.*, 2013, **219**, 537–544.

161 Y. Peng, Y. Zhang, H. Huang and C. Zhong, *Chem. Eng. J.*, 2018, **333**, 678–685.

162 P. W. Seo, N. A. Khan and S. H. Jhung, *Chem. Eng. J.*, 2017, **315**, 92–100.

163 M. R. Azhar, H. R. Abid, V. Periasamy, H. Sun, M. O. Tade and S. Wang, *J. Colloid Interface Sci.*, 2017, **500**, 88–95.

164 T. Qian, Y. Zhang, J. Cai, W. Cao, T. Liu, Z. Chen, J. Liu, F. Li and L. Zhang, *J. Colloid Interface Sci.*, 2021, **603**, 582–593.

165 S. Zhao, S. Li, Z. Zhao, Y. Su, Y. Long, Z. Zheng, D. Cui, Y. Liu, C. Wang and X. Zhang, *Environ. Sci. Pollut. Res.*, 2020, **27**, 39186–39197.

166 Q. Wu, H. Yang, L. Kang, Z. Gao and F. Ren, *Appl. Catal., B*, 2020, **263**, 118282.

167 X. Fang, S. Wu, Y. Wu, W. Yang, Y. Li, J. He, P. Hong, M. Nie, C. Xie, Z. Wu, K. Zhang, L. Kong and J. Liu, *Appl. Surf. Sci.*, 2020, **518**, 146226.

168 F. Wei, Q. Ren, H. Zhang, L. Yang, H. Chen, Z. Liang and D. Chen, *RSC Adv.*, 2021, **11**, 9977–9984.

169 Y. Kong, Y. Zhuang, K. Han and B. Shi, *Colloids Surf., A*, 2020, **588**, 124360.

170 L. Wang, X. Cui, J. Xu, G. Wang, M. Guo, L. Yu, K. Yang, Z. Luo, A. Zeng and G. Chen, *J. Pharm. Biomed. Anal.*, 2022, **219**, 114933.

171 S.-W. Lv, J.-M. Liu, C.-Y. Li, N. Zhao, Z.-H. Wang and S. Wang, *Catal. Sci. Technol.*, 2020, **10**, 4703–4711.

172 G. C. C. Yang and P.-L. Tang, *Water Sci. Technol.*, 2016, **73**, 2268–2274.

173 S. Radmehr, M. Hosseini Sabzevari, M. Ghaedi, M. H. Ahmadi Azqhandi and F. Marahel, *J. Environ. Chem. Eng.*, 2021, **9**, 105975.

174 Y. Gao, Y. Li, L. Zhang, H. Huang, J. Hu, S. M. Shah and X. Su, *J. Colloid Interface Sci.*, 2012, **368**, 540–546.

175 L. A. Al-Khateeb, S. Almotiry and M. A. Salam, *Chem. Eng. J.*, 2014, **248**, 191–199.

176 Y. Tang, H. Guo, L. Xiao, S. Yu, N. Gao and Y. Wang, *Colloids Surf., A*, 2013, **424**, 74–80.

177 K. Balasubramani, N. Sivarajasekar and M. Naushad, *J. Mol. Liq.*, 2020, **301**, 112426.

178 W. T. Tee, N. Y. L. Loh, B. Y. Z. Hiew, P. L. Show, S. Hanson, S. Gan and L. Y. Lee, *J. Environ. Manage.*, 2023, **344**, 118363.

179 S. J. Segovia-Sandoval, L. M. Pastrana-Martínez, R. Ocampo-Pérez, S. Morales-Torres, M. S. Berber-Mendoza and F. Carrasco-Marín, *Sep. Purif. Technol.*, 2020, **237**, 116341.

180 W. K. Wakejo, A. Maged, B. T. Meshesha, J. W. Kang, A. G. Demesa, S. Chakrabarti, T. Bhaskar, A. K. Gupta and A. Bhatnagar, *Colloids Surf., A*, 2024, **681**, 132718.

181 C. F. Varela, L. C. Moreno-Aldana and Y. Y. Agámez-Pertuz, *J. Bioresour. Bioprod.*, 2024, **9**, 58–73.

182 H. Ashebir, J. F. Nure, A. Worku and T. A. M. Msagati, *Desalination Water Treat.*, 2024, **320**, 100691.

183 I. Quesada-Peñate, C. Julcour-Lebigue, U.-J. Jáuregui-Haza, A.-M. Wilhelm and H. Delmas, *Chem. Eng. J.*, 2009, **152**, 183–188.

184 L. Sun, S. Wan, D. Yuan and Z. Yu, *Sci. Total Environ.*, 2019, **664**, 24–36.

185 L. Lu, M. Liu, Y. Chen and Y. Luo, *R. Soc. Open Sci.*, 2021, **8**, 210336.

186 L. Limousy, I. Ghouma, A. Ouederni and M. Jeguirim, *Environ. Sci. Pollut. Res.*, 2017, **24**, 9993–10004.

187 D. Naghipour, L. Hoseinzadeh, K. Taghavi, J. Jaafari and A. Amouei, *Int. J. Environ. Anal. Chem.*, 2023, **103**, 5706–5719.

188 S. Dutta, M. Walden, A. Sinelshchikova, R. Ettlinger, E. Lizundia and S. Wuttke, *Adv. Funct. Mater.*, 2024, **34**(52), 2410751.

189 A.-N. Parvulescu and S. Maurer, *Front. Chem.*, 2022, **10**, DOI: 10.3389/fchem.2022.1050363.

190 P. Zhang, X. Tan, S. Liu, Y. Liu, G. Zeng, S. Ye, Z. Yin, X. Hu and N. Liu, *Chem. Eng. J.*, 2019, **378**, 122141.

191 R. Rusmin, B. Sarkar, T. Tsuzuki, N. Kawashima and R. Naidu, *Chemosphere*, 2017, **186**, 1006–1015.

192 H. J. An, B. N. Bhadra, N. A. Khan and S. H. Jhung, *Chem. Eng. J.*, 2018, **343**, 447–454.

193 M. Toński, M. Paszkiewicz, J. Dołżonek, M. Flejszar, A. Bielicka-Giełdoń, P. Stepnowski and A. Białk-Bielińska, *Colloids Surf., A*, 2021, **618**, 126355.

194 S. A. Baig, J. Zhu, N. Muhammad, T. Sheng and X. Xu, *Biomass Bioenergy*, 2014, **71**, 299–310.

195 H. Patel, *J. Saudi Chem. Soc.*, 2021, **25**, 101302.

196 L. Yang, Z. Zhou, L. Xiao and X. Wang, *Environ. Sci. Technol.*, 2003, **37**, 5057–5061.

197 A. O. C. Iroegbu, M. L. Teffo, E. R. Sadiku, R. Meijboom and S. P. Hlangothi, *npj Clean Water*, 2025, **8**, 85.

198 H. Kaur, N. Devi, S. S. Siwal, W. F. Alsanie, M. K. Thakur and V. K. Thakur, *ACS Omega*, 2023, **8**, 9004–9030.

199 H. Wang, Y. Hao, Q. Liu, R. Han, X. Lu, C. Song, D. Ma, N. Ji and C. Liu, *J. Environ. Chem. Eng.*, 2022, **10**, 108737.

200 S.-Y. Pan, Y.-Y. Hsiao, S. Negi, B. M. Matsagar and K. C.-W. Wu, *ACS Sustain. Chem. Eng.*, 2024, **12**, 17793–17805.

201 D. Pryce, A. M. E. Khalil and F. A. Memon, *Sci. Total Environ.*, 2022, **817**, 152985.

202 H. Fu, L. Gutierrez, S. Shewfelt, Y. Xiong and K. A. Gray, *Water Res.*, 2024, **261**, 121998.

203 U. C. Rajesh, J. Wang, S. Prescott, T. Tsuzuki and D. S. Rawat, *ACS Sustain. Chem. Eng.*, 2015, **3**, 9–18.

204 J. O. Ighalo, F. O. Omoarukhe, V. E. Ojukwu, K. O. Iwuozor and C. A. Igwegbe, *Cleaner Chemical Engineering*, 2022, **3**, 100042.

205 E. A. Serna-Galvis, J. Arboleda-Echavarría, A. Echavarría-Isaza and R. A. Torres-Palma, *Environ. Sci. Pollut. Res.*, 2024, **31**, 63427–63457.

206 A. Maity and V. Polshettiwar, *ACS Appl. Nano Mater.*, 2018, **1**, 3636–3643.

207 A. Saroa, A. Singh, N. Jindal, R. Kumar, K. Singh, P. Guleria, R. Boopathy and V. Kumar, *Bioengineered*, 2023, **14**(1), DOI: 10.1080/21655979.2023.2260919.

208 S. Feijoo, S. González-García, Y. Moldes-Diz, C. Vazquez-Vazquez, G. Feijoo and M. T. Moreira, *J. Clean. Prod.*, 2017, **143**, 528–538.

209 A. Lucchesi Schio, M. R. Farias Soares, G. Machado and T. Barcellos, *ACS Sustain. Chem. Eng.*, 2021, **9**, 9661–9670.

210 J. Shaheen, Y. H. Fseha and B. Sizirici, *Heliyon*, 2022, **8**, e12388.

211 S. Nand, P. P. Singh, S. Verma, S. Mishra, A. Patel, S. Shukla and P. K. Srivastava, *Sci. Total Environ.*, 2025, **966**, 178743.

212 J. Lehmann, A. Cowie, C. A. Masiello, C. Kammann, D. Woolf, J. E. Amonette, M. L. Cayuela, M. Camps-Arbestain and T. Whitman, *Nat. Geosci.*, 2021, **14**, 883–892.

213 D. Gamaralalage, S. Rodgers, A. Gill, W. Meredith, T. Bott, H. West, J. Alce, C. Snape and J. McKechnie, *Biochar*, 2025, **7**, 50.

214 N. Bhutia, P. Adhikari and N. Dutta, *Biotechnological Interventions in the Removal of Emerging Pollutants*, 2025, 301–320.

215 S. Kim, C. M. Park, A. Jang, M. Jang, A. J. Hernández-Maldonado, M. Yu, J. Heo and Y. Yoon, *J. Membr. Sci.*, 2019, **570–571**, 77–84.

216 L. Yang, Z. Zhou, L. Xiao and X. Wang, *Environ. Sci. Technol.*, 2003, **37**, 5057–5061.

217 S. Waqas, N. Y. Harun, N. S. Sambudi, M. R. Bilad, K. J. Abioye, A. Ali and A. Abdulrahman, *Water*, 2023, **15**, 1913.

218 D. Micale, C. Ferroni, R. Uglietti, M. Bracconi and M. Maestri, *Chem. Ing. Tech.*, 2022, **94**, 634–651.

219 F. K. Tominaga, N. F. Boiani, T. T. Silva, V. S. G. Garcia and S. I. Borrely, *Chemosphere*, 2022, **309**, 136671.

220 M. Paredes-Laverde, J. Silva-Agredo and R. A. Torres-Palma, *J. Environ. Manage.*, 2018, **213**, 98–108.

221 R. Changotra, H. Rajput and A. Dhir, *J. Photochem. Photobiol., A*, 2019, **376**, 175–184.

222 N. Rosman, W. N. W. Salleh, M. A. Mohamed, J. Jaafar, A. F. Ismail and Z. Harun, *J. Colloid Interface Sci.*, 2018, **532**, 236–260.

223 S. Patel, S. Mondal, S. K. Majumder, P. Das and P. Ghosh, *ACS Omega*, 2020, **5**, 32305–32317.

224 E. Ferrer-Polonio, J. Fernández-Navarro, M.-I. Iborra-Clar, M.-I. Alcaina-Miranda and J. A. Mendoza-Roca, *J. Environ. Manage.*, 2020, **263**, 110368.

225 C. Echevarría, C. Valderrama, J. L. Cortina, I. Martín, M. Arnaldos, X. Bernat, A. De la Cal, M. R. Boleda, A. Vega, A. Teuler and E. Castellví, *J. Clean. Prod.*, 2020, **273**, 123108.